Naval Research Laboratory
Washington, DC 20375-5000 NRL Memorandum Report 5830 July 29, 1986

Input Impedance of an Infinite Linear Scanned Array of Flat Rectangular Strips Inside a Dielectric Loaded Parallel Plate Waveguide

S. N. SAMADDAR

Electromagnetics Branch
Radar Division

SECURITY CLASSIFICATION OF THIS PAGE

REPORT DOCUMENTATION PAGE

1a REPORT SECURITY CLASSIFICATION UNCLASSIFIED	1b RESTRICTIVE MARKINGS
2a SECURITY CLASSIFICATION AUTHORITY	3. DISTRIBUTION/AVAILABILITY OF REPORT Approved for public release; distribution unlimited.
2b DECLASSIFICATION/DOWNGRADING SCHEDULE	
4 PERFORMING ORGANIZATION REPORT NUMBER(S) NRL Memorandum Report 5830	5. MONITORING ORGANIZATION REPORT NUMBER(S)
6a NAME OF PERFORMING ORGANIZATION Naval Research Laboratory 6b. OFFICE SYMBOL (If applicable) 5371	7a. NAME OF MONITORING ORGANIZATION
6c. ADDRESS (City, State, and ZIP Code) Washington, DC 20375-5000	7b. ADDRESS (City, State, and ZIP Code)
8a. NAME OF FUNDING/SPONSORING ORGANIZATION Office of Naval Research 8b. OFFICE SYMBOL (If applicable)	9. PROCUREMENT INSTRUMENT IDENTIFICATION NUMBER
8c. ADDRESS (City, State, and ZIP Code) Arlington, VA 22217	10. SOURCE OF FUNDING NUMBERS PROGRAM ELEMENT NO. 61153N; PROJECT NO.; TASK NO. RR021-05-43; WORK UNIT ACCESSION NO. DN380-049

11 TITLE (Include Security Classification)
Input Impedance of an Infinite Linear Scanned Array of Flat Rectangular Strips Inside a Dielectric Loaded Parallel Plate Waveguide

12. PERSONAL AUTHOR(S)
Samaddar, S.N.

13a. TYPE OF REPORT	13b. TIME COVERED FROM ____ TO ____	14. DATE OF REPORT (Year, Month, Day)	15. PAGE COUNT
		1986 July 29	59

16. SUPPLEMENTARY NOTATION

17 COSATI CODES		
FIELD	GROUP	SUB-GROUP

18. SUBJECT TERMS (Continue on reverse if necessary and identify by block number)
Input impedance; Monopoles; Waveguide; S-band
(continues)

19. ABSTRACT (Continue on reverse if necessary and identify by block number)

Impedance variation as a function of H-plane scan angles of an infinite linear array of flat rectangular monopoles (strips) inside a dielectric loaded parallel plate waveguide is studied both theoretically and experi- mentally in the S-band frequencies. In theoretical analysis simplified along the probes (monopole strips) and neglect of the effect of the gap at the junction of a probe and its coaxial feed line, were made. It is found that this simplified theory can predict qualitatively the experimental data of interest, such as input impedance. Both theory and experiments show that a dielectric slab with a relatively low dielectric constant (1.3) inserted in an appropriate manner can improve the bandwidth and impedance performance of the array. Certain experimental results show a bandwidth of about 28% with respect to the center frequency 3.5 GHz, having a VSWR <2.

Another interesting result is the relation between the width W of a flat rectangular probe and the radius ρ of a circular probe situated similarly inside two identical rectangular waveguides. The probe impedances or VSWR's for these situations are found to be the same, respectively, for all practical purposes when $W = 4.882\,\rho$, which was obtained numerically representing a correction to the electrostatic result $W = 4\rho$ found by Wheeler.

20 DISTRIBUTION/AVAILABILITY OF ABSTRACT ☒ UNCLASSIFIED/UNLIMITED ☐ SAME AS RPT ☐ DTIC USERS	21. ABSTRACT SECURITY CLASSIFICATION UNCLASSIFIED
22a NAME OF RESPONSIBLE INDIVIDUAL S.N. Samaddar	22b TELEPHONE (Include Area Code) 202/767-6277; 22c. OFFICE SYMBOL 5371

DD FORM 1473, 84 MAR 83 APR edition may be used until exhausted. All other editions are obsolete

SECURITY CLASSIFICATION OF THIS PAGE

18. SUBJECT TERMS (Continued)

Parallel plate waveguide
Variational expression
Scan angle
Bandwidth
Dielectric loaded
VSWR
H-plane

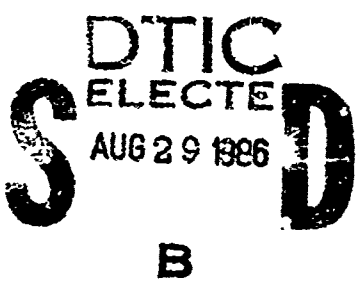

CONTENTS

INPUT IMPEDANCE OF AN INFINITE LINEAR SCANNED ARRAY OF FLAT RECTANGULAR STRIPS INSIDE A DIELECTRIC LOADED PARALLEL PLATE WAVEGUIDE

I. INTRODUCTION

In most phased array studies the main objective has been to achieve a wide angle impedance match, preferably with a wide bandwidth. Different configurations and techniques have been proposed for this purpose. For instance, Magill and Wheeler [1], and also Munk with his co-workers [2] proposed different dielectric loading for achieving wide-angle impedance match. The geometry of the problem can play an important role in satisfying some requirements. For example, a parallel plate waveguide can be used advantageously to study the H-plane and E-plane scans independently. With these general objectives of wide-angle and wideband H-plane performance, this paper is aimed at deriving an analytical expression for the input impedance of an infinite linear array of flat rectangular probes (monopoles) inside a dielectric loaded parallel plate waveguide using some simplifying assumptions, so that theoretical results can predict the corresponding experimental data reasonably. The parallel plate waveguide is short circuited at a distance $z = -L$ from the array of probes [Fig. 1]. The monopoles are flat rectangular strips fed from coaxial lines. The most difficult point of this kind of analysis is in the determination of the current distribution along the probes. This can be done, in principle, by solving an integral equation, which involves a tedious task of numerical computations. In order to alleviate this difficulty, it has become common to assume a sinusoidal current distribution along a current element [2]-[7]. This, one of the simplifying assumptions used here, is

Manuscript approved May 27, 1986.

an approximation and, therefore, any theoretical analysis based on this can only approximately predict the corresponding experimental results. Another simplifying assumption consists of neglecting the effect of the gap at the junction between the probe and its coaxial feed line [4,5]. One of the results of this study is, therefore, to find how much agreement between these approximate theoretical results and the corresponding experimental data is achieved. This will be shown mainly through graphical display.

With the above objectives and assumptions in mind, a mathematical formulation of the problem which includes several dielectric sheets, is presented in section II. In section III, a sinusoidal current distribution is introduced and then the unknown complex amplitudes of the field components are determined. A method to improve the accuracy of this current distribution by using the stationary property of the input impedance is also discussed. A theoretical expression for the input impedance of the infinite linear array of the probes is derived in section IV. In section V, various special cases, including the correspondence between the infinite linear array and its equivalent simulators, are discussed. Various theoretical and experimental results obtained from different sources are compared in section VI. This section also includes the comparison between theoretical and experimental results of the input impedance of an infinite linear array of flat rectangular probes inside a parallel plate waveguide loaded with and without dielectric sheets. Experiments were performed using several waveguide simulators. However, results involving only one simulator are presented for economy of space. It was found that the theory based on the simplifying assumptions mentioned earlier can predict the general or qualitative behavior of input

impedance or VSWR. It has also been shown that a dielectric sheet with a relatively low dielectric constant can improve the bandwidth and match of the array. Munk and his coworkers [2] had also shown that a sheet of low dielectric constant can improve scanning characteristics. The relative position between the dielectric slab and the array chosen in ref. [2] is, however, different from that considered here. The frequency range used for this investigation was about 3.0 GHz to 4.0 GHz, over which the experimental data show a good impedance match. This frequency range indicates a bandwidth of 28% with respect to the center frequency 3.5 GHz having VSWR <2. The corresponding theoretical result shows somewhat lower bandwidth.

II. MATHEMATICAL FORMULATION OF THE PROBLEM

The geometry of the problem is shown in Fig. 1. It consists of a parallel plate waveguide of width b and short circuited at a distance z=-L from an infinite linear array of y-directed flat rectangular probes (or monopole) located in the plane z=0. In the positive z direction, the waveguide extends to infinity. The probes are separated a distance a in the x-direction. All elements (i.e., probes) of the array are excited with equal amplitude. The phase shift per unit length is a constant h, which is a function of frequency and scan angle. In this formulation, it is assumed that the array is inside a dielectric slab with relative dielectric constant ε_2, which again is sandwiched between two other slabs having relative dielectric constants ε_1 and ε_3, respectively. These dielectric slabs are included for better matching. The primary reason for choosing flat rectangular probe, instead of circular, is for achieving better bandwidth. Since the width of the probe is very small compared to the wavelength in the medium in which the probe is embedded, the current

in the probe can be assumed to be confined to the y-direction (along the length of the probe) only. The electromagnetic field satisfies the following time harmonic Maxwell's equations.

$$\nabla \times \vec{E} = -j\omega\mu_o \vec{H} \tag{1}$$

$$\nabla \times \vec{H} = j\omega\varepsilon_o\varepsilon_i \vec{E} + \hat{y}_o J_y \tag{2}$$

where $\hat{y}_o$ is the unit vector in the y-direction. The relative dielectric constant ε_i is a piecewise constant having different values, in general, in different regions of the z-dimension. The assumed harmonic time dependence $\exp(j\omega t)$ is suppressed for convenience. The effect of the gap at the junction between a probe and its coaxial feed is neglected.

The x-dependent part of the current on the probe array can be represented by an infinite number of delta functions in the following way.

$$\sum_{n=-\infty}^{\infty} e^{-jhna}\delta(x-x'-na) \tag{2a}$$

where the factor $\exp(-jhna)$ represents the uniform phase shift in the x-direction. Since the expression (2a) is a periodic function, it can also be represented by a Fourier-series of the following form.

$$\sum_{n=-\infty}^{\infty} e^{-jhna}\delta(x-x'-na) = \frac{1}{a} \sum_{n=-\infty}^{\infty} e^{-j(h+\frac{2\pi n}{a})(x-x')} \tag{2b}$$

The right-hand side of (2a) implies that the x-dependence of the fields will also have a similar infinite series representation containing a factor $\exp[-j(h+2n\pi/a)x]$. It may be noted that this expression is also

equivalent to a Floquet mode [7] or an unnormalized mode function associated with a one dimensional grating [8].

Since the electric current is in the y-direction, in absence of any dielectric slab the electromagnetic field could have been expressed in terms of a single component A_y of a vector potential $\vec{A}$ [4]. However, this approach is not valid in the present situation where dielectric slabs are present. Therefore, a more general method, namely modal analysis [8] appropriate for a linear infinite array will be adopted here. In this method, let us introduce two transverse scalar mode functions, $\phi_{nm}(x,y)$ and $\psi_{nm}(x,y)$. The word transverse means x,y-dimensions (which is perpendicular to the propagation direction z). These functions are defined by

$$\phi_{nm}(x,y) = \left(\frac{2}{ab}\right)^{1/2} \cdot \frac{1}{K_{tnm}} \cdot e^{-jK_{xn}x} \sin\left(\frac{m\pi y}{b}\right) \tag{3a}$$

$$\psi_{nm}(x,y) = \left(\frac{2-\delta_{om}}{ab}\right)^{1/2} \cdot \frac{1}{K_{tnm}} e^{-jK_{xn}x} \cos\left(\frac{m\pi y}{b}\right) \tag{3b}$$

where

$$\delta_{om} = \begin{cases} 1 \text{ when } m=0 \\ 0 \text{ when } m\neq 0 \end{cases} \tag{3c}$$

$$K_{xn} = h + 2n\pi/a \tag{3d}$$

$$K_{tnm} = \left[K_{xn}^2 + (m\pi/b)^2\right]^{1/2} \tag{3e}$$

Note that the functions given by (3a) and (3b) have the same x-dependence shown in (2b). Furthermore, $\phi_{nm}(x,y)$ and $\frac{\partial}{\partial y}\psi_{nm}(x,y)$ vanish at $y = o$ and $y = b$. Define two vector functions by

$$\vec{\phi}_{nm}(x,y) = - \nabla_t \phi_{nm}(x,y) \tag{4a}$$

$$\vec{\psi}_{nm}(x,y) = -\nabla_t \psi_{nm}(x,y) \tag{4b}$$

where $\nabla_t = \hat{x}_o \frac{\partial}{\partial x} + \hat{y}_o \frac{\partial}{\partial y}$, $\hat{x}_o$ and $\hat{y}_o$ are unit vectors in the respective coordinate directions. Note that $\vec{\phi}_{nm}(x,y)$ and $\vec{\psi}_{nm}(x,y)$ have the following properties.

$$\nabla_t \nabla_t \cdot \vec{\phi}_{nm}(x,y) = -K_{tnm}{}^2 \vec{\phi}_{nm}(x,y) \tag{5a}$$

$$\nabla_t \cdot [\vec{\phi}_{nm}(y,x) \times \hat{z}_o] = 0 \tag{5b}$$

$$\nabla_t \nabla_t \cdot \vec{\psi}_{nm}(x,y) = -K_{tnm}{}^2 \vec{\psi}_{nm}(x,y) \tag{6a}$$

$$\nabla_t \cdot [\vec{\psi}_{nm}(x,y) \times \hat{z}_o] = 0 \tag{6b}$$

where $\hat{z}_o$ is the unit vector in the z-direction.

$$\iint \vec{\phi}_{nm}(x,y) \cdot \vec{\phi}^*_{n',m'}(x,y)\, dxdy = \delta_{nn'}\delta_{mm'} \tag{7a}$$

$$\iint \vec{\psi}_{nm}(x,y) \cdot \vec{\psi}^*_{n',m'}(x,y)\, dxdy = \delta_{nn'}\delta_{mm'} \tag{7b}$$

$$\iint \vec{\phi}_{nm}(x,y) \cdot \hat{z}_o \times \vec{\psi}^*_{n',m'}(x,y) dxdy = 0 \tag{7c}$$

The asterisk signs in (7a) to (7c) indicate respective complex conjugates. The symbols $\delta_{nn'}$ and $\delta_{mm'}$ represent Kronecker delta functions with the usual meaning. The region of integration in (7a) to (7c) is the

unit cell, i.e., $-\frac{a}{2} \leq x \leq \frac{a}{2}$ and $o \leq y \leq b$. With these orthonormal vector mode functions $\vec{\phi}_{nm}(x,y,)$ and $\vec{\Psi}_{nm}(x,y,)$, the complete electromagnetic field can be represented in the following manner [8]:

$$\vec{E}_t(\vec{r}) = \sum_{n=-\infty}^{\infty} \sum_{m=o}^{\infty} V_{nm}^{TM}(z)\vec{\phi}_{nm}(x,y) + \sum_{n=-\infty}^{\infty} \sum_{m=o}^{\infty} V_{nm}^{TE}(z)\vec{\Psi}_{nm}(x,y)x\hat{z}_o \quad (8a)$$

$$\vec{H}_t(\vec{r}) = \sum_{n=-\infty}^{\infty} \sum_{m=o}^{\infty} I_{nm}^{TM}(z)\hat{z}_o x\vec{\phi}_{nm}(x,y) + \sum_{n=-\infty}^{\infty} \sum_{m=o}^{\infty} I_{nm}^{TE}(z)\vec{\Psi}_{nm}(x,y) \quad (8b)$$

$$j\omega\varepsilon_o\varepsilon_i E_z(\vec{r}) = \sum_{n=-\infty}^{\infty} \sum_{m=o}^{\infty} I_{nm}^{TM}(z)K_{tnm}^2\phi_{nm}(x,y) \quad (8c)$$

$$j\omega\mu_o H_z(\vec{r}) = \sum_{n=-\infty}^{\infty} \sum_{m=o}^{\infty} V_{nm}^{TE}(z)K_{tnm}^2\psi_{nm}(x,y) \quad (8d)$$

The subscripts t and z denote transverse (i.e., x,y) and z components of the respective field vectors. The functions $V_{nm}^{TM}(z)$ and $I_{nm}^{TM}(z)$ are the modal voltage and current amplitudes for TM waves. Similarly, $V_{nm}^{TE}(z)$ and $I_{nm}^{TE}(z)$ belong to the TE-type waves. Adopting the procedures similar to that in ref. [8], it can be shown that these modal voltage and current amplitudes obey the following transmission line differential equations.

$$-\frac{d}{dz} V_{nm}^{TM}(z) = \Gamma_{inm} Z_{inm}^{TM} I_{nm}^{TM}(z) \quad (9a)$$

$$-\frac{d}{dz} I_{nm}^{TM}(z) = \Gamma_{inm} Y_{inm}^{TM} V_{nm}^{TM}(z) + \iint_S \hat{y}_o \cdot \vec{\phi}_{nm}^*(x,y)J_y(\vec{r})dxdy \quad (9b)$$

$$-\frac{d}{dz} V_{nm}^{TE}(z) = j\omega\mu_o I_{nm}^{TE}(z) = \Gamma_{inm} Z_{inm}^{TE} I_{nm}^{TE}(z) \tag{10a}$$

$$-\frac{d}{dz} I_{nm}^{TE}(z) = \Gamma_{inm} Y_{inm}^{TE} V_{inm}^{TE}(z) - \iint_S \hat{x}_o \cdot \vec{\Psi}^*_{nm}(x,y) J_y(\vec{r}) dxdy \tag{10b}$$

where

$$\Gamma_{inm} = [K_{tnm}^2 - K_o^2 \varepsilon_i]^{1/2} \tag{11a}$$

$$K_o = \omega \sqrt{\mu_o \varepsilon_o} \tag{11b}$$

$$i = 1,2,3 \text{ and } 4 \tag{11c}$$

$$Z_{inm}^{TE} = 1/Y_{inm}^{TE} = j\omega\mu_o/\Gamma_{inm} = \text{modal impedance for TE-waves} \tag{11d}$$

$$Z_{inm}^{TM} = 1/Y_{inm}^{TM} = \Gamma_{inm}/j\omega\varepsilon_o\varepsilon_i = \text{modal impedance for TM-waves} \tag{11e}$$

$$J_y(\vec{r}) = \frac{I(y)}{W} \delta(z) = \hat{J}_y(y)\delta(z) \tag{12}$$

$$\text{for } |x| \leq \frac{W}{2} \text{ and } o \leq y \leq d$$

W = width of the flat rectangular probe in the x direction

d = effective length of the probe.

Note that the probe is infinitely thin in the z dimension. The integrations in (9b) and 10b) are over the surface of the probe as defined in (12). The propagation constant Γ_{inm} given by (11a) is different in different regions and when it is real, the corresponding waves are evanescent. For propagating modes (such as main beam and grating lobes) Γ_{inm} is purely imaginary. For convenience, let us introduce U_{nm}^{TE} and U_{nm}^{TM} defined respectively by

$$U_{nm}^{TE} = j\omega\mu_o \iint_s \hat{x}_o \cdot \vec{\psi}^*_{nm}(x,y) \frac{I(y)}{W} dxdy \tag{13a}$$

and

$$U_{nm}^{TM} = -\frac{\Gamma_{2nm}^2}{j\omega_o\varepsilon_o\varepsilon_2} \iint_s \hat{y}_o \cdot \vec{\phi}^*_{nm}(x,y) \frac{I'(y)}{W} dxdy \tag{13b}$$

In order to solve for $V_{nm}^{TM}(z)$, $I_{nm}^{TM}(z)$, $V_{nm}^{TE}(z)$, and $I_{nm}^{TE}(z)$, it is convenient to obtain a second order differential equation for each $V_{nm}^{TM}(z)$ and $V_{nm}^{TE}(z)$. This can be done by eliminating $I_{nm}^{TM}(z)$ and $I_{nm}^{TE}(z)$ from (9a), (9b) and (10a), (10b). The results are (using (12), (13a) and (13b)

$$\left(\frac{d^2}{dz^2} - \Gamma_{inm}^2\right) V_{nm}^{TM}(z) = -U_{nm}^{TM}\delta(z) \tag{14a}$$

and

$$\left(\frac{d^2}{dz^2} - \Gamma_{inm}^2\right) V_{nm}^{TE}(z) = -U_{nm}^{TE}\delta(z) \tag{14b}$$

These two equations must be solved subject to the following boundary conditions.

At the source (i.e., at z=o)

$$V_{nm}^{TM}(z=o^+) = V_{nm}^{TM}(z=o^-) \tag{15a}$$

$$\frac{d}{dz} V_{nm}^{TM}(z=o^+) - \frac{d}{dz} V_{nm}^{TM}(z=o^-) = -U_{nm}^{TM} \tag{15b}$$

$$V_{nm}^{TE}(z=o^+) = V_{nm}^{TE}(z=o^-) \tag{16a}$$

$$\frac{d}{dz} V_{nm}^{TE}(z=o^+) - \frac{d}{dz} V_{nm}^{TE}(z=o^-) = -U_{nm}^{TE} \tag{16b}$$

Since there is no other sources, $V_{nm}^{TM}(z)$, $I_{nm}^{TM}(z)$, $V_{nm}^{TE}(z)$ and $I_{nm}^{TE}(z)$ are continuous at $z = -\ell_2$, δ_s and $\delta_s + \delta_3$. $I_{nm}^{TM}(z)$ and $I_{nm}^{TE}(z)$ can be determined from $V_{nm}^{TM}(z)$ and $V_{nm}^{TE}(z)$, respectively, via Eqs. (9a) and (10a). In addition, $V_{nm}^{TE}(z)$ and $V_{nm}^{TM}(z)$ must vanish at $z = -L$. For $z>\delta_s+\delta_3$, $V_{nm}^{TE}(z)$ and $V_{nm}^{TM}(z)$ behave like outgoing waves.

The solutions of (14a) and (14b) subject to the boundary conditions discussed above can now be expressed in the following manner.

$$V_{nm}^{TM}(z) = \begin{cases} A_{nm}^{TM} \sinh\{\Gamma_{1nm}(z+L)\} & -L \le z \le -\ell_2 \quad (17a) \\ B_{1nm}^{TM}[\exp(\Gamma_{2nm}z) - \hat{R}_{eff}^{11}(nm)\cdot\exp\{-\Gamma_{2nm}(2\ell_2+z)\}], & -\ell_2 \le z \le o \quad (17b) \\ B_{2nm}^{TM}[\exp(-\Gamma_{2nm}z) + R_{eff}^{11}(n,m)\cdot\exp\{-\Gamma_{2nm}(2\delta_s - z)\}, & o \le z \le \delta_s \quad (17c) \\ C_{nm}^{TM}[\exp(-\Gamma_{3nm}z) + R_{3,4}^{11}(n,m)\cdot\exp\{-\Gamma_{3nm}(2\delta_s + 2\delta_3 - z)\}], & \delta_s \le z \le \delta_s + \delta_3 \quad (17d) \\ D_{nm}^{TM}\exp(-\Gamma_{4nm}z) & z \ge \delta_s + \delta_3 \quad (17e) \end{cases}$$

$$V_{nm}^{TE}(z) = \begin{cases} A_{nm}^{TM}\sinh\{\Gamma_{1nm}(z+L)\} & -L \le z \le -\ell_2 \quad (18a) \\ B_{1nm}^{TE}[\exp(\Gamma_{2nm}z) - \hat{R}_{eff}^{\perp}(n,m)\cdot\exp\{-\Gamma_{2nm}(2\ell_2+z)\}], & -\ell_2 \le z \le o \quad (18b) \\ B_{2nm}^{TE}[\exp(-\Gamma_{2nm}z) + R_{eff}^{\perp}(n,m)\cdot\exp\{-\Gamma_{2nm}(2\delta_s - z)\}], & o \le z \le \delta \quad (18c) \\ C_{nm}^{TE}[\exp(-\Gamma_{3nm}z) + R_{3,4}^{\perp}(n,m)\cdot\exp\{-\Gamma_{3nm}(2\delta_s + 2\delta_3 - z)\}], & \delta_s \le z \le \delta_s + \delta_3 \quad (18d) \\ D_{nm}^{TE}\exp(-\Gamma_{4nm}z) & (18e) \end{cases}$$

$$\hat{R}^{11}_{eff}(n,m)=[R^{11}_{1,2}(n,m)+\exp\{-2\Gamma_{1nm}(L-\ell_2)\}]/[1+R^{11}_{1,2}(n,m)\cdot\exp\{-2\Gamma_{1nm}(L-\ell_2\}]$$

(19a)

$$R^{11}_{1,2}(n,m)=(\varepsilon_1\Gamma_{2nm}-\varepsilon_2\Gamma_{1nm})/(\varepsilon_1\Gamma_{2nm}+\varepsilon_2\Gamma_{1nm}) \tag{19b}$$

$$R^{11}_{eff}(n,m)=[R^{11}_{2,3}(n,m)+R^{11}_{3,4}(n,m)\cdot\exp(-2\Gamma_{3nm}\delta_3)]/[1+R^{11}_{2,3}(n,m)\cdot R^{11}_{3,4}(n,m)\cdot$$

$$\cdot\exp\{-2\Gamma_{3nm}\delta_3\}] \tag{19c}$$

$$R^{11}_{2,3}(n,m)=(\varepsilon_2\Gamma_{3nm}-\varepsilon_3\Gamma_{2nm})/(\varepsilon_2\Gamma_{3nm}+\varepsilon_3\Gamma_{2nm}) \tag{19d}$$

$$R^{11}_{3,4}(n,m)=(\varepsilon_3\Gamma_{4nm}-\Gamma_{3nm})/(\varepsilon_3\Gamma_{4nm}+\Gamma_{3nm}) \tag{19e}$$

$$B^{TM}_{1nm}=\frac{U^{TM}_{nm}}{2\Gamma_{nm}}[1+R^{11}_{eff}(n,m)\cdot\exp(-2\Gamma_{2nm}\delta_s)]/[1+\hat{R}^{11}_{eff}(n,m)\cdot R^{11}_{eff}(n,m)\cdot$$

$$\cdot\exp\{-2\Gamma_{2nm}(\ell_2+\delta_s)\}] \tag{19f}$$

$$B^{TM}_{2nm}=B^{TM}_{1nm}\cdot[1-\hat{R}^{11}_{eff}(n,m)\cdot\exp(-2\Gamma_{2nm}\ell_2)]/[1+R^{11}_{eff}(n,m)\cdot\exp(-2\Gamma_{2nm}\delta_s)] \tag{19g}$$

$$A^{TM}_{nm}=B^{TM}_{1nm}\cdot\varepsilon_2\Gamma_{1nm}\cdot\exp(-\Gamma_{2nm}\ell_2)[1+\hat{R}^{11}_{eff}(n,m))]/[\varepsilon_1\Gamma_{2nm}\cosh\{\Gamma_{1nm}(L-\ell_2)]$$

(19h)

$$C^{TM}_{nm}=B^{TM}_{2nm}\cdot\exp\{-\delta_s(\Gamma_{2nm}-\Gamma_{3nm})\}\cdot[1+R^{11}_{eff}(n,m)]/[1+R^{11}_{3,4}(n,m)\cdot\exp\{-2\Gamma_{3nm}\delta_3\}]$$

(19i)

$$D_{nm}^{TM} = [1+R_{3,4}^{11}(n,m)]\cdot\exp\{(\ell_s+\delta_3)(\Gamma_{4nm}-\Gamma_{3nm})]\}\cdot C_{nm}^{TM} \qquad (19j)$$

$$\hat{R}_{eff}^{\perp}(n,m) = [R_{1,2}^{\perp}(n,m) + \exp\{-2\Gamma_{1nm}(L-\ell_2)\}]/[1+R_{1,2}^{\perp}(n,m)\cdot \cdot \exp\{-2\Gamma_{1nm}(L-\ell_2)\}] \qquad (20a)$$

$$R_{1,2}^{\perp}(n,m) = (\Gamma_{1nm}-\Gamma_{2nm})/(\Gamma_{1nm}+\Gamma_{2nm}) \qquad (20b)$$

$$R_{eff}^{\perp}(n,m) = [R_{2,3}^{\perp}(n,m)+R_{3,4}^{\perp}(n,m)\cdot\exp(-2\Gamma_{3nm}\delta_3)]/[1+R_{2,3}^{\perp}\cdot R_{3,4}^{\perp}(n,m)\cdot \cdot\exp(-2\Gamma_{3nm}\delta_3)] \qquad (20c)$$

$$R_{2,3}^{\perp}(n,m) = (\Gamma_{2nm}-\Gamma_{3nm})/(\Gamma_{2nm}+\Gamma_{3nm}) \qquad (20d)$$

$$R_{3,4}^{\perp}(n,m) = (\Gamma_{3nm}-\Gamma_{4nm})/(\Gamma_{3nm}+\Gamma_{4nm}) \qquad (20e)$$

$$B_{1nm}^{TE} = \frac{U_{nm}^{TE}}{2\Gamma_{2nm}}[1+R_{eff}^{\perp}\cdot\exp(-2\Gamma_{2nm}\delta_s)]/[1+\hat{R}_{eff}^{\perp}(n,m)\cdot R_{eff}^{\perp}(n,m)\cdot \cdot\exp\{-2\Gamma_{2nm}(\ell_2+\delta_s)\}] \qquad (20f)$$

$$B_{2nm}^{TE} = B_{1nm}^{TE}\cdot[1-\hat{R}_{eff}^{\perp}(n,m)\cdot\exp(-2\Gamma_{2nm}\ell_2)]/[1+R_{eff}^{\perp}(n,m)\cdot\exp(-2\Gamma_{2nm}\delta_s)] \qquad (20g)$$

$$A_{nm}^{TE} = B_{1nm}^{TE} \cdot \Gamma_{2nm} \cdot \exp(-\Gamma_{2nm}\ell_2)[1+\hat{R}^{\perp}_{eff}(n,m)]/[\Gamma_{1nm}\cosh\{\Gamma_{1nm}(L-\ell_2)\}] \tag{20h}$$

$$C_{nm}^{TE} = B_{2nm}^{TE} \cdot \exp\{-\delta_s(\Gamma_{2nm}-\Gamma_{3nm})\} \cdot [1+R^{11}_{eff}(n,m)]/[1+R^{\perp}_{3,4}(n,m) \cdot \exp(-2\Gamma_{3nm}\delta_3)] \tag{20i}$$

$$D_{nm}^{TE} = [1+R^{\perp}_{3,4}(n,m)] \cdot \exp\{(\delta_s+\delta_3)(\Gamma_{3nm}-\Gamma_{4nm})\} \cdot C_{nm}^{TE} \tag{20j}$$

III. PROBE CURRENT DISTRIBUTION

The amplitude factors U_{nm}^{TE} and U_{nm}^{TM} given by (13a) and (13b) which depend on the current distribution on the probe still remain unknown. In reality, it is difficult to calculate the exact current distribution in an environment shown in Fig. 1. Therefore, various approximate methods are sought. For example, one may assume a known current distribution [3,4, 5,6] which has been found to be valid in some situations. For a probe this current distribution is taken to be $\sin[K(d-y)]$, where d is the length of the probe, y is the coordinate along which the current varies and K is the free space wave number of the surrounding medium. If b is the height of the waveguide in the y-direction, it has also been shown experimentally [5,6] that theoretical results based on the assumption of this sinusoidal current are in good agreement with those of experimental for $d \leq .6b$ and $d \leq \lambda/4$, where $\lambda = 2\pi/K$. On the other hand, if the probe is at the interface between two media with propagation constants K_1 and K_2, then the effective current distribution may be taken [9] as $\sin[K_e(d-y)]$, where $K_e = \sqrt{K_1^2 + K_2^2}$, assuming that the permeability is the same for both media. All these results are, of course, derived for an antenna in an otherwise free space.

Another approach to derive an approximate form of current distribution follows from the stationary property of the input inpedance of the probe with respect to the current distribution. It is shown [4,10] that the input impedance of a probe can be cast into a variational form with respect to the variation of current distribution in the probe. Then the current distribution may be expressed in terms of two or more arbitrary parameters which are computed by requiring that the partial derivative of the input impedance with respect to each of these unknown parameters vanishes. When the expression for the input impedance is too complex, this procedure becomes tedious.

Most of the theoretical models deal with idealized situations. For example, for a probe, one may assume a current distribution either as a known function or a trial function having a few arbitrary parameters. Even an integral equation for the current may be set up using an idealized probe geometry. However, in actual practice, the probe geometry comprising the coaxial feed system differs from the idealized theoretical configuration. As a result, the actual current may depart substantially from the theoretically computed one. Therefore, in order to minimize the complexity in theoretical computation, the following approach will be chosen here.

The current distribution on the probe will be assumed to be known and has the following form (see Eq. 12).

$$I(y) = I_o \sin[K_e(d-y)] \qquad (21)$$

$$o \leq y \leq d, \quad |x| \leq W/2$$

where K_e is the effective propagation constant. If the medium in which the probe is embedded has a relative dielectric constant ε_2, then $K_e = \omega\sqrt{\mu_o\varepsilon_o\varepsilon_2} = K_o\sqrt{\varepsilon_2}$. On the other hand, if the probe lies at the interface between two media with relative dielectric constants ε_i and ε_j, then $K_e = K_o\sqrt{(\varepsilon_i+\varepsilon_j)/2}$.

Using now (21), the amplitude factors U_{nm}^{TE} and U_{nm}^{TM} can be calculated from Eqs. (13a) and (13b). The results are:

$$U_{nm}^{TE} = -2I_o\omega\mu_o K_e \sin^2\left(\frac{K_{ed}}{2}\right)\left(\frac{2-\delta_{om}}{ab}\right)^{1/2}\left(\frac{K_{xn}}{K_{tnm}}\right)\frac{S_n F_{em}}{\hat{K}_{em}^2} \tag{22a}$$

$$U_{nm}^{TM} = -\frac{2I_o K_e}{j\omega\varepsilon_o\varepsilon_2}\,\Gamma_{2nm}^2 \cdot \sin^2\left(\frac{K_{ed}}{2}\right)\left(\frac{2}{ab}\right)^{1/2} \cdot \left(\frac{m\pi/b}{K_{tnm}}\right)\frac{S_n F_{em}}{\hat{K}_{em}^2} \tag{22b}$$

$$F_{em} = 1 - \sin^2(m\pi d/2b)/\sin^2(K_e d/2) \tag{23a}$$

$$S_n = \sin(K_{xn}W/2)/(K_{xn}W/2) \tag{23b}$$

$$\hat{K}_{em}^2 = (m\pi/b)^2 - K_e^2 \tag{23c}$$

IV. INPUT IMPEDANCE OF THE INFINITE LINEAR ARRAY OF PROBES

The input impedance Z_{in} is defined [3,4] by the ratio of the complex power radiated by the probe and the mean square input current, i.e.,

$$Z_{in} = -\frac{1}{2}\iint_s \vec{E}_t(x,y,z=o)\cdot\hat{y}\ \hat{J}_y^*(y)ds/[\tfrac{1}{2}|\hat{J}(o)|^2] \ . \qquad (24)$$

The integration is over the probe surface inside the unit cell containing the origin. $\hat{J}_y(y)$ is given by (12) and (21). The electric field $\vec{E}_t(x,y,z=o)$ can be calculated from (8a) using (17c), (18c), (19g), (20g), (22a), and (22b). Carrying out the indicated operations in (24), the input impedance Z_{in} can be expressed as

$$Z_{in} = \frac{jZ_oK_oK_e^2}{2ab}\tan^2(K_ed/2)\sum_{n=-\infty}^{\infty}\sum_{m=o}^{\infty}\frac{(2-\delta_{om})}{\Gamma_{2nm}}\left(\frac{K_{xn}}{K_{tnm}}\right)^2\left(\frac{F_{em}S_n}{\hat{K}_{em}^2}\right)^2 T_{nm}^{\perp}$$

$$-\frac{jZ_oK_e^2}{abK_o\varepsilon_2}\tan^2(K_ed/2)\sum_{n=\infty}^{\infty}\sum_{m=o}^{\infty}\left(\frac{m\pi/b}{K_{tnm}}\right)^2\Gamma_{2nm}\left(\frac{F_{em}S_n}{\hat{K}_{em}^2}\right)^2\cdot T_{nm}^{11} \qquad (24a)$$

where

$$T_{nm}^{\perp} = \frac{[1+R_{eff}^{\perp}(n,m)\cdot\exp(-2\Gamma_{2nm}\delta_s)][1-\hat{R}_{eff}^{\perp}(n,m)\cdot\exp(-2\Gamma_{2nm}\ell_2)]}{[1+R_{eff}^{\perp}(n,m)\ \hat{R}_{eff}^{\perp}(n,m)\cdot\exp\{-2\Gamma_{2nm}(\ell_2+\delta_s)\}]} \qquad (24b)$$

$$T_{nm}^{11} = \frac{[1+R_{eff}^{11}(n,m)\cdot\exp(-2\Gamma_{2nm}\delta_s)][1-\hat{R}_{eff}^{11}(n,m)\cdot\exp(-2\Gamma_{2nm}\ell_2)]}{[1+R_{eff}^{11}(n,m)\cdot\hat{R}_{eff}^{11}(n,m)\cdot\exp\{-2\Gamma_{2nm}(\ell_2+\delta_s)\}]} \qquad (24c)$$

$$Z_o = \sqrt{\mu_o/\varepsilon_o} \ . \qquad (24d)$$

Phased arrays are generally designed in such a way that only the lowest order mode or the main beam (for which n=o=m in (24a)) propagates. However, due to dielectric loading the first few higher order modes (i.e., grating lobes, such as when n=±1, m=o; n=o, m=1, etc.) may become propagating waves inside a dielectric layer. Even in this case, Γ_{inm} is real for large values of n and m (which represent evanescent modes). Therefore, for large values of n and m, both $T^{\perp}_{nm}$ and T^{11}_{nm} tend to approach unity.

From Eqs. (3d), (3e), (11a), and 23a) to (23c), one finds that K_{xn}, K_{tnm} and Γ_{inm} behave like n as n tends to infinity for a fixed m. On the other hand, for a finite value of W, S_n is on the order of 1/n as $n\to\infty$. When n remains fixed and m becomes very large K_{tnm} and Γ_{inm} tend to m. F_{em} and $\hat{K}^2_{em}$ approach unity and m^2, respectively, as m assumes a large value. From this observation, it follows that the first term (double series) of (24a) converges like $1/n^3$ and $1/m^7$ as n and m tend to infinity, respectively. The second term of (24a), however, converges like $1/n^3$ and $1/m^3$ as n and m approach infinity, respectively. On the otherhand, if $(K_{xn}W)$ is very small, the impedance series converges slowly with respect to n.

V. SPECIAL CASES

A. IN ABSENCE OF ANY DIELECTRIC SLAB

In this case $\varepsilon_1 = \varepsilon_2 = \varepsilon_3 = \varepsilon_4 = 1$

$$\Gamma_{inm} = \Gamma_{nm} = \sqrt{K_{tnm}^2 - K_c^2}\ , \quad i = 1,2,3,4$$

$$R^{\perp}_{eff}(n,m) = R^{11}_{eff}(n,m) = o$$

$$\hat{R}^{\perp}_{eff}(n,m) = \hat{R}^{11}_{eff}(n,m) = \exp\{-2\Gamma_{nm}(L-\ell_2)\}$$

$$T^{\perp}_{nm} = T^{11}_{nm} = 1 - \exp(-2\Gamma_{nm}L)$$

$$Z_{in} = \frac{jZ_o K_o K_e^2}{2ab} \tan^2(K_e d/2) \sum_{n=-\infty}^{\infty} \sum_{m=o}^{\infty} \frac{(2-\delta_{om})}{\Gamma_{nm}} \left(\frac{K_{xn}}{K_{tnm}}\right)^2 \left(\frac{F_{em} S_n}{K^2_{em}}\right)^2 [1-\exp(-2\Gamma_{nm}L)]$$

$$- \frac{-jZ_o K_o}{ab} \tan^2(K_e d/2) \sum_{n=-\infty}^{\infty} \sum_{m=o}^{\infty} \left(\frac{m\pi/b}{K_{tnm}}\right)^2 \Gamma_{nm} \left(\frac{F_{em} S_n}{K^2_{em}}\right)^2 [1-\exp(-2\Gamma_{nm}L)] \quad . \quad (25)$$

In this case, K_e may be taken as $K_o = \omega\sqrt{\mu_o \varepsilon_o}$. In the absence of any short circuit at $z = -L$, one may take $e^{-2\Gamma_{nm}L} = o$. This is justified by taking the limit $L \to \infty$, with the assumption that $Re\Gamma_{nm} > c$ for all n and m. For propagating modes, this assumption implies inclusion of slight loss in the medium.

B. PROBE AT THE CENTER OF THE BROAD FACE OF A RECTANGULAR WAVEGUIDE

In Fig. 1, a is taken to be the distance between the consecutive probes of a linear array in the x-dimension. This is also shown in Fig. 2a for convenience. The width of the parallel plate waveguide is b in the y-dimension. In this special case, the rectangular waveguide has dimensions a and b in the x and y directions, respectively.

The center of the probe is at x=a/2. This probe at the center of a rectangular waveguide is equivalent to a linear array of probes whose adjacent elements are 180° out of phase in a parallel plate waveguide as shown in Fig. 2b. This observation follows from image theory. Therefore, when the uniform phase shift h associated with the probes in Fig. 1 or

Fig. 2a, is given the value π/a, the problem of Fig. 1 becomes equivalent to that in a rectangular waveguide with a probe at the center, $x = \frac{a}{2}$. As a result, the following transformations take place.

$$K_{xn} = h + 2n\pi/a = (2n+1)\pi/a \tag{26a}$$

$$K_{tnm} = \left[K_{xn}^2 + (m\pi/b)^2\right]^{1/2} = \left[\{(2n+1)\pi/a\}^2 + (m\pi/b)^2\right]^{1/2} \tag{26b}$$

$$\Gamma_{inm} = \left[\{(2n+1)\pi/a\}^2 + (m\pi/a)^2 - K_o^2\varepsilon_i\right]^{1/2} . \tag{26c}$$

It can readily be seen from (24a) to (24c) and (26a) to (26c) that the argument of the summation with respect to n associated with the input impedance Z_{in} becomes then a function of $(2n+1)^2$. If it is assumed that G is a function of $(2n+1)^2$, then it can be shown easily that

$$\sum_{n=-\infty}^{\infty} G[(2n+1)^2] = 2 \sum_{n=o}^{\infty} G[(2n+1)^2] . \tag{27}$$

Using this information, the desired input impedance of a centrally located rectangular probe in a rectangular waveguide is given by

$$Z_{in} = \frac{jZ_o K_o K_e^2}{ab} \tan^2(K_e d/2) \sum_{n=o}^{\infty} \sum_{m=o}^{\infty} \frac{(2-\delta_{om})}{\Gamma_{2nm}} \left(\frac{K_{xn} F_{em} S_n}{K_{tnm} \hat{K}_{em}^2} \right)^2 T_{nm}^{\perp}$$

$$- \frac{j2Z_o K_e^2 \tan^2(K_e d/2)}{ab\, K_o \varepsilon_2} \sum_{n=o}^{\infty} \sum_{m=1}^{\infty} \left(\frac{(m\pi/b) F_{em} S_n}{K_{tnm} \hat{K}_{em}^2} \right)^2 \Gamma_{2nm} T_{nm}^{11} . \qquad (28)$$

In (28) the relations (26a) to (26c) are to be used.

The relation (28) can further be specialized for the situation when there is no dielectric slabs inside the rectangular waveguide, i.e., when $\varepsilon_1 = \varepsilon_2 = \varepsilon_3 = \varepsilon_4 = 1$. Following the procedure described in Section V-A, we have the desired expression obtained from (28).

$$Z_{in} = \frac{jZ_o K_o^3}{ab} \tan^2(K_o d/2) \sum_{n=o}^{\infty} \sum_{m=o}^{\infty} \frac{(2-\delta_{om})}{\Gamma_{nm}} \left(\frac{K_{xn} F_{em} S_n}{K_{tnm} \hat{K}_{em}^2} \right)^2 [1-\exp(-2\Gamma_{nm} L]$$

$$- \frac{j2Z_o K_o}{ab} \tan^2(K_o d/2) \sum_{n=o}^{\infty} \sum_{m=1}^{\infty} \left(\frac{(m\pi/b) F_{em} S_n}{K_{tnm} \hat{K}_{em}^2} \right)^2 \Gamma_{nm} [1-\exp(-2\Gamma_{nm} L)] \qquad (29)$$

The Eq. (29) can be simplified to the following form.

$$Z_{in} = \frac{-jZ_o K_o}{ab} \tan^2(K_o d/2) \sum_{n=o}^{\infty} \sum_{m=o}^{\infty} \frac{(2-\delta_{om})}{\Gamma_{nm}} \left(\frac{F_{em} S_n}{\hat{K}_{em}} \right)^2 [1-\exp(-2\Gamma_{nm} L)] \qquad (30)$$

It may be noted that situations represented by Eqs. (28) and (29) or (30) correspond to a particular scan angle for a given frequency.

C. SOME SIMULATOR MODELS

Since it is very expensive and time consuming to build a periodic array with a large number of elements for experimental testing and measurements, use of simulator models, which are simple in structure and contain only a few elements, has been proposed and proved to be successful [11,12]. The principle involved in this simulation is also discussed in these references [11,12] and, therefore, will not be repeated here. One of the restrictions in simulator application is that each simulator represents only one sample of scan conditions in the actual array. Consequently, several simulators are generally built for a study of a given array. For example, the special case discussed in section V-B consisting of a rectangular waveguide with a probe at the center, represents a particular scan condition defined by $h=K_o\sin\theta=\pi/a$ for the array problem depicted in Fig. 1. The H-plane scan condition for this infinite linear array can be simulated approximately by the simple TE_{10} mode in a rectangular waveguide. The number of elements N, to be placed in the rectangular waveguide and the broad dimension a of this guide depend again on the scan angle θ, satisfying the condition

$$\begin{aligned} h &= K_o\sin\theta = \pi/a \\ \text{or} \quad \sin\theta &= \lambda/2a \end{aligned} \tag{31a}$$

If d_x is the interelement spacing, then the number of elements required for a given scan angle is approximately given by

$$N = a/d_x = \frac{\lambda}{2d_x \sin\theta} \quad . \tag{31b}$$

For a given scan angle, say $\theta=35°$, the required broad dimension of the rectangular waveguide is $a=0.8717\lambda$. If d_x is chosen as $d_x=0.575\lambda$, then $N=a/d_x=1.516$. Thus, the approximate number of elements is 1.5, i.e., one element is bisected by one wall of the guide (in the x-direction) and the other element is placed at a distance $d_x=2a/3$ from that bisecting wall. Since the bisected element is short circuited by the wall, it is observed that its existence (or non-existence) has no effect. This observation then implies that a rectangular waveguide with a probe at a distance 2a/3 from one wall, $a=0.877\lambda$ being the broad dimension of the guide, when excited by the TE_{10} mode, simulates the scan condition ($\theta=35°$) of an infinite array of probes in a parallel plate waveguide. For making this observation more instructive, the input impedance of an off-centered probe in a rectangular waveguide is computed (see Appendix) separately and the corresponding numerical results are compared with the appropriate situations for an infinite array probe, for which Eq. (25) has been used. The equivalence between any other simulator and the infinite linear array in a parallel plate waveguide for a given scan condition can be explained similarly [9,10].

VI. DISCUSSIONS OF NUMERICAL AND EXPERIMENTAL RESULTS

Over the past several decades to the present, numerous theoretical and experimental investigations of phased arrays composed of electric dipoles or monopoles have been made. In theoretical analysis a knowledge of the current distribution along these dipoles or monopoles is essential. However, it is not known a priori. It can be determined in principle by solving an integral equation for the current. Once the current distribution is determined, other parameters of interest (such as input impedance, VSWR, radiation pattern, etc.) can be computed from the

knowledge of the current. The solution of the integral equation involving current is generally accomplished numerically. Since this procedure is tedious and time consuming, one generally assumes a sinusoidal current distribution in theoretical analyses for simplicity. Although such an assumption simplifies the analysis considerably, differences are expected to exist between the theoretical and the corresponding experimental results. Nevertheless, this simplified assumption may be considered satisfactory, provided the theoretical results can predict at least the qualitative behavior of the input impedance and other observables of practical interest, so that the experimental results can be better understood. This is one of the objectives of this theoretical study. It may be noted that for some problems [5,6] assumption of known sinusoidal current distribution produced theoretical results which were in good agreement with those of the corresponding experiments.

Before we proceed to make a comparison between various theoretical and experimental results, let us digress for a moment in order to present the interesting result to be discussed in the next section.

VI. A. CONNECTION BETWEEN CIRCULAR AND FLAT RECTANGULAR PROBE IMPEDANCE OR VSWR

One may choose either a circular probe or a flat rectangular probe for a phased array composed of monopoles. A question then arises whether there is a simple connection between two corresponding observables of the same kind (such as input impedance of the probe, VSWR, etc.). This information is particularly important when some results (theoretical or experimental) using one kind of probe are known, then how the theoretical or experimental, as the case may be, parameters for the other kind of the probe may be chosen so that the two corresponding results should be the

same. It appears that H.A. Wheeler* was also interested in this matter and derived a relation using conformal mapping of fields in an unpublished report. Wheeler's relation is W=4P where W is the width of an infinitely thin flat rectangular probe and ρ is the radius of the circular probe, other parameters of the two configurations (one with the flat rectangular probe and the other with the circular probe) remaining the same. The implication of this relation may be interpreted by using the following example. Suppose there are two identical rectangular waveguides, one with a circular probe of radius ρ and the other with a flat rectangular probe of width W=4P. These probes are of the same length, excited in the same manner and situated in an identical manner in their respective waveguides. Then the input impedance, VSWR, etc., of the two situations are expected to be the same. Since Wheeler's relation is based on conformal mapping, valid for electrostatic fields, it may not be satisfactory in the microwave region. This observation turns out to be true. Although Wheeler's relation is very simple, in a frequency dependent situation no such closed form relation can be established. Therefore, one shall have to resort to numerical computations. In order to obtain such a relation let us consider a known result [4] of a circular probe, as shown in Fig. 3, at the center of the broadface of a rectangular waveguide. The waveguide is short circuited at a distance z= -L from the axis of the probe. When only the fundamental TE_{10} mode is propagating, the input impedance of the probe is given by [4] the following expression. It may be recalled that in this case also the current distribution on the probe is assumed to be known and is the same as in eq. (21).

---

* This information was communicated to the author by Dr. W. K. Kahn.

$$Z_{in} = \frac{2Z_o \tan^2(K_o d/2)}{ab\beta K_o} \sin^2(\beta L) + \frac{jZ_o \tan^2(K_o d/2)}{2\pi K_o b} \left[\ln\left(\frac{2a}{\pi\rho}\right) + \frac{0.0518 K_o^2 a^2}{\pi^2}\right.$$

$$\left. + \frac{2\pi}{\beta a} \cdot \sin(2\beta L) - 2\left(1 - \frac{2\rho}{a}\right) - 2K_o^2 \sum_{m=1}^{\infty} F_{em}^2 K_o(\hat{K}_{em}\rho)/\hat{K}_{em}^2\right] , \qquad (32)$$

where $K_e = K_o$ and $\beta = [K_o^2 - (\pi/a)^2]^{1/2}$. F_{em}, $\hat{K}_{em}$ and Z_o are defined by (23a), (23c) and (24d), respectively. $K_o(\hat{k}_{em}\rho)$ is the modified Bessed function of the second kind, of order zero. In the absence of the short circuit (i.e., $L \to \infty$) the corresponding expression for the input impedance of the probe can be shown to have the following form.

$$Z_{in} = \frac{Z_o \tan^2(K_o d/2)}{ab\beta K_o} + \frac{jZ_o \tan^2(K_o d/2)}{2\pi K_o b} \left[\ln\left(\frac{2a}{\pi\rho}\right) + \frac{0.0518 K_o^2 a^2}{\pi^2}\right. \qquad (33)$$

$$\left. - 2\left(1 - \frac{2\rho}{a}\right) - 2K_o^2 \cdot \sum_{m=1}^{\infty} F_{em}^2 K_o(\hat{K}_{em}\rho)/\hat{K}_{em}^2\right]$$

The result corresponding to eq.(32) for a flat reccangular probe is given by (30). In the absence of any short circuit the input impedance can be obtained from (30) by letting $\exp(-2\Gamma_{nm}L) = 0$. Numerical values of these impedance expressions are obtained using the parameters, a = 6.0 cm, b = 3.4036 cm, L = 2.21234 cm and ∞, d = 1.651 cm, 1.75 cm and 1.90 cm. The radius ρ of the circular probe is kept fixed at 0.127 cm. However, the

width W of the flat rectangular probe is varied from 4ρ to 5ρ. The results are shown in Fig. 3a thru 4c in the form of VSWR as a function of frequency. The voltage standing wave ratio (VSWR) is computed from the relation

$$VSWR = \left[1 + \frac{|Z_{in}/50 - 1|}{|Z_{in}/50 + 1|}\right] \Big/ \left[1 - \frac{|Z_{in}/50 - 1|}{|Z_{in}/50 + 1|}\right] \tag{34}$$

It is found from these numerical results that the input impedance and VSWR of a circular probe remain practically unchanged when it is replaced by a flat rectangular one, provided that $W = 4.882\rho$, other parameters being the same. This relation should not be considered exact. It may change with frequency, length of the probe, distance L of the short circuit, etc. These observations are based on the numerical results shown in Fig. 3a thru 4c. However, the relation $W = 4.882\rho$ appears to be adequate for the frequency range and other parameters considered here. For the purpose of comparison, the VSWR corresponding to Wheeler's relation $W = 4\rho$ is also presented. Although Wheeler's relation is obtained by using conformal mapping, valid for electrostatic fields, results (such as impedance, VSWR, etc.) obtained by using his relation approach closer to those obtained by using the relation $W = 4.882\rho$, when the frequency is higher and the probe length is longer.

The relationship $W = 4.882\rho$ implies that the expressions for the input impedances of flat rectangular probes developed in this paper for various situations can also be used for the corresponding cases where the former probe is replaced by a circular one of radius W/4.882. It is, of course, assumed that other parameters remain unchanged.

VI. B. A CIRCULAR PROBE IN AN INFINITELY LONG RECTANGULAR WAVEGUIDE WITHOUT SHORT CIRCUIT

Before presenting our experimental and theoretical results for the linear array of flat rectangular monopoles in a parallel plate waveguide or its equivalent simulator, let us first make a comparison between some experimental and theoretical results related to Collin's [4] and Al-Hakkak's [5] model, since their various assumptions are similar to ours. This model consists of a circular probe, fed from a coaxial waveguide in an infinitely long rectangular waveguide without short circuit. The main reasons for choosing this model here are the following:

1. The theoretical results can easily be derived from Collin's work [4] with a minor modification. This was done by Al-Hakkak [5], who also performed experiments and compared with the theory.
2. The theoretical results for this model can also be obtained approximately from our theory for a simulator using the relation $W = 4.882\rho$ in eq. A-10 in view of the finding in the previous section.

Although Chang and Kahn [6] studied a similar problem using a flat rectangular stub inside an infinitely long rectangular waveguide without using any coaxial feed line, their experimental and theoretical results cannot be used here directly for comparison. This model does not have any problem of gap at the coax junction.

The theoretical expression for the input impedance is given in eq. (33), which is a slight modification of the result given by Collin [4]. In view of the relation discussed in section VI-A, the numerical values of eq. (33) for a given probe radius ρ can also be obtained approximately from eq. (A-10) with $W = 4.882\rho$, and the omission of the exponential

factor in (A-10), other parameters remaining the same. For the use of eq. (33), it should be remembered that only the fundamental TE_{10} mode is propagating. In addition, the theory does not take into account the gap (or aperture) at the junction of the probe and the coaxial connector and assumes a known sinusoidal current distribution along the probe. A further limitation of the theory is the assumption that the diameter of the probe is very small compared to the wavelength. In ref. [5], Al-Hakkak finds also that the length of the probe d should be such that $d<0.6b$ and $d<\lambda/4$, where b is the shorter dimension of the broadface of the waveguide. Chang and Khan [6] also discussed these limitations of the theory. It may be noted again that the sinusoidal current distribution assumed here and in refs. [4,5] is also used by Stark [3] among others for similar theoretical study of phased array antennas having monopole or dipoles as elements.

Figures (5a), (5b) and (5c) show some theoretical and experimental values of normalized (with respect to 50Ω) input impedance of circular probes having three different diameters, but of the same length in an infinitely long rectangular waveguide without short circuit. Although the parameter c, the outer diameter of the coaxial line, does not enter into the theory due to the approximation made, it does affect experimental results. The probes are located at the center of the broadface of the waveguide. The results show a general agreement between the theory and the experiment. The main reasons for the existence of difference between the theoretical and experimental results may be attributed to the gap (or aperture effect) and the assumption of a sinusoidal current distribution along the probe. In order to observe the effect of the gap alone, the probe was removed from the coaxial connector in an experiment. It was

then noticed that there was hardly any transmission of energy through the gap into the waveguide (showing extremely high VSWR). This phenomenon might have been known also to others and, perhaps, motivated them to neglect the effect of the gap in similar theoretical works as a good approximation. This may not be justified since, when the gap and the probe are present simultaneously, the field distribution at the junction is altered due to the coupling between the gap and the probe. In addition, the combined effect of the gap and the probe diameters appears to play a role. For example, an increase in probe diameter causes an increase in the input impedance and thereby improves VSWR. An increase in the probe diameter is also associated with a decrease in the resonance frequency (at which the input impedance is real) of the system. This was also observed by Al-Hakkak [5]. It is also observed (not presented here) both theoretically and experimentally that an increase in probe length d improves the VSWR within a limited frequency band. It may be noted also that at frequencies above 4.22 GHz, the chosen probe length d = 1.778 cm does not satisfy the condition $d<\lambda/4$.

In spite of all these restrictions made in the theory, Al-Hakkak's experimental results are surprisingly in good agreement with the theory. Figure 6d shows theoretical results corresponding to the parameters used by Al-Hakkak [5]. These are essentially Al-Hakkak's results (recomputed). The agreement is so close that the experimental and theoretical results are not shown separately in Fig. 5d. It may be mentioned here that Chang and Khan [6] also obtained good agreement between their theory and experiments in which there is no gap effect. Their theory is also similar to that of Collin's where use of known sinusoidal current distribution is made. Note that Chang and Khan [6] apparently determined the actual

current distribution by solving an integral equation numerically. They found that the actual current distribution, so determined, does not differ much from a sinusoidal current distribution provided $d<\lambda/4$.

The results of this section may be considered as precursors of what can be expected of the results for the linear array of monopoles in a parallel plate waveguide and hence may be used for guidance. The experimental results, Figs. 5a to 5c, were generated in our laboratory.

VI. C. INPUT IMPEDANCE OF AN INFINITE LINEAR ARRAY OF FLAT RECTANGULAR MONOPOLES INSIDE A PARALLEL PLATE WAVEGUIDE

In this case, eqs. (24a) and A-8) are used for theoretical computations. Equation (24a) is valid for both the presence and absence of a dielectric slab and for all scan angles. On the other hand, eq. (A-8) is used for the case without any dielectric and for those scan angles and frequencies shown in Fig. 6a. In the presence of a dielectric slab only, the eq. (24a) is used with $\varepsilon_1=1=\varepsilon_2=\varepsilon_4$, $\varepsilon_3=1.3$, $a=2.84\cdot(2.54)\text{cm}=3d_1$, where $2.84\cdot(2.54)$cm is the longer dimension of the broadface of the simulator waveguide, d_1 is the offset distance of the center of the probe from one end of the simulator waveguide [Fig. A-1], $b=1.34\cdot(2.54)$cm, $W=0.2\cdot(2.54)$cm, $d=0.702\cdot(2.54)$cm, $L=0.863\cdot(2.54)$cm, $\delta_s=0.984\cdot(2.54)$cm, $\delta_3=1.0\cdot(2.54)$cm. All the measurements were taken using a simulator (Fig. A-1) with $3d_1$=its longer dimension of the broadface. Note that a of Fig. 1 is not the same as a of Fig. A-1. In the absence of any dielectric, eqs. (24a) and (A-8) provide identical results, subject to the condition $d_1=2.84\cdot(2.54)$ cm/3=distance between the consecutive probes of the array in the parallel plate waveguide. This is, of course, expected.

Figure 6b shows the theoretical and experimental results in the absence of any dielectric slab. Here also, the theoretical and experimental results are in qualitative agreement. Similar results with a

dielectric slab (ε_3=1.3) are shown in Fig. 6c. The experimental results show a tuning effect in the presence of the dielectric slab. Although this effect is not pronounced in the theoretical result; it indicates such an effect qualitatively. It may be noted that the experimental results show better bandwidth and match than the corresponding theoretical results. Some theoretical computations (not presented here) also show that the bandwidth and match can be improved to some extent by decreasing the inter-element spacing a. The reasons for the difference between the theoretical and experimental results are the same as those discussed in the previous section VI.B. It should now be apparent that discussions and presentation of theoretical and experimental results in section VI.B provide better understanding of the results of this section.

VII. CONCLUSIONS

For theoretical analysis of problems consisting of electric dipole or monopole elements, it is common practice to assume a sinusoidal current distribution along such current elements. This is done mainly to simplify the complexity of the problem. Although such an assumption is inaccurate, it can predict qualitatively expected behaviors of various experimental results (input impedance, VSWR, etc.). These expectations were illustrated by comparing theoretical and experimental results obtained here and from previously published literature. It was one of the aims of the present study to make such comparisons. The primary causes of the difference between the theoretical and experimental results are explained.

In addition, certain experimental results show a better bandwidth (about 28%) and match than the corresponding simplified theoretical results. It is also shown both theoretically and experimentally, that a slab of low dielectric constant (such as 1.3, 1.4) properly placed in

front of the array, can improve the bandwidth and VSWR at wide scan angles. Munk and his coworkers [2] had also shown that a sheet of low dielectric constant can improve scanning characteristics. The relative position between the dielectric slab and the array chosen in ref. [2] is, however, different from that considered here. The frequency range used for this study is about 3.0 GHz to 4.0 GHz.

Another interesting result is the relation between the width W of a flat rectangular probe and the radius ρ of a circular probe situated similarly inside two identical rectangular waveguides. The probe impedances and VSWR's for these two situations are found to be the same for all practical purposes when W is properly related to ρ. The proper relation found here is $W=4.882\rho$ for a given set of waveguide parameters and frequencies. This factor was obtained numerically representing a correction to the electrostatic result $W=4\rho$ found by Wheeler.

It may be observed from this study insofar as the simplified theory is concerned, that it provides results relatively easily, and does correctly indicate the trend of the experimental results.

ACKNOWLEDGEMENT

The author wishes to take this opportunity to express his appreciation to Professor Walter K. Kahn for numerous discussions, to Mr. Allen Miller for his able assistance in obtaining numerical results, and to Mr. Billy Wright who provided the experimental data. He also acknowledges the receipt of the manuscript of the paper, "Array of Coaxially-Fed Monopole Elements in a Parallel Plate Waveguide," by Dr. B. Tomasic and Professor A. Hessel. It arrived so late that the author was unable to make any comparison here.

REFERENCES

1. E.G. Magill and H.A. Wheeler, "Wide-angle Impedance Matching of a Planar Array Antenna by a Dielectric Sheet," IEEE Trans. Antennas and Propagation, Vol. AP-14, 49-53, Jan 1966.

2. B.A. Munk, T.W. Kornbau and R.D. Fulton, "Scan Independent Phased Arrays," Radio Science, Vol. 14, No. 6, pp. 979-990, Nov-Dec 1979.

3. L. Stark, "Radiation Impedance of a Dipole in an Infinite Planar Phased Array," Radio Science, Vol. 1 (New Series), No. 3, pp. 361-377, Mar 1966.

4. R.E. Collin, "Field Theory of Guided Waves", New York: McGraw-Hill, 1960, Ch. 7.

5. M.J. Al-Hakkak, "Experimental investigation of the input-impedance characteristics of an antenna in a rectangular waveguide," Electron. Letters, Vol. 5, pp. 513-514, Oct 16, 1969.

6. K. Chang and P.J. Khan, "Analysis of a Narrow Capacitive Strip in Waveguide," IEEE Trans. Microwave Theory Tech., Vol. MTT-19, pp. 295-308, Mar 1971.

7. R.E. Collin, "Field Theory of Guided Waves," New York: McGraw-Hill, 1960, pp. 368-371.

8. N. Marcuvitz, "Waveguide Handbook," New York; McGraw-Hill, 1951, Chapt. 1 and pp. 88-89.

9. B.L. Coleman, "Propagation of Electromagnetic Disturbances Along a Thin Wire in a Horizontally Stratified Medium," Phil. Mag. Vol 41, pp. 276-288, 1950.

10. L.Levin, "Advanced Theory of Waveguides," London, England: Iliffe 1951.

11. P.W. Hannan and M.A. Balfour, "Simulation of a Phased Array Antenna in Waveguide," IEEE Trans. Antennas Propagation AP-13, pp 342-353, May 1965.

12. A.A. Oliner and R.G. Malech, "Simulation of Infinite Arrays by Waveguide," Hansen (ed.) Microwave Scanning Antennas, Vol. 2, Array Theory and Practice, Academic Press, pp. 322-335, 1966.

APPENDIX

RADIATION FROM AN OFF-CENTERED PROBE INSIDE A RECTANGULAR WAVEGUIDE SHORT CIRCUITED AT A DISTANCE L FROM THE PROBE

The geometry of the situation is shown in Fig. A-1. It consists of a rectangular waveguide of dimension a and b ($a \geq b$) and short circuited at a distance $z = -L$ from an off-centered flat rectangular probe of length d and width w. The axis of the y-directed probe lies at $x = d_1$ and $z = o$. In the positive z-direction, the waveguide extends to infinity. For simplicity, it is assumed that there are no dielectric slabs inside the waveguide. The current distribution is the same as given by (21). Although one can use a method similar to that presented in section 2, the absence of any dielectric permits one to use only a single component of the vector potential $\vec{A}$. Since the current is directed along y, one finds $\vec{A} = \hat{y}_o A_y$. Then it can be shown that

$$\vec{E} = -j\omega\vec{A} + \nabla\nabla\cdot\vec{A}/(j\omega\varepsilon_o\mu_o) \tag{A-1a}$$

$$\vec{H} = \nabla\times\vec{A}/\mu_o \tag{A-1b}$$

Therefore,

$$E_y = (1/j\omega\mu_o\varepsilon_o)\left[K_o^2 + \frac{\partial^2}{\partial y^2}\right] A_y \tag{A-2a}$$

$$(\nabla^2 + K_o^2)A_y = -\mu_o J_y \tag{A-2b}$$

Let us construct a Green's function $G(\vec{r},\vec{r}')$ which satisfies the following differential equation and boundary conditions [4].

$$(\nabla + K_o^2)G(\vec{r},\vec{r}') = \delta(x-x')\delta(y-y')\delta(z)$$

$$\vec{r} = (x,y,z) \text{ and } \vec{r}' = (x',y',o) \tag{A-3}$$

$$G = o \text{ at } x=o,a \text{ and } z=-L$$

$$\partial G/\partial y = o \text{ at } y=o,b \tag{A-4}$$

G also satisfies radiation condition at $z=\infty$.

Then

$$A_y = -\mu_o \iint_S G(\vec{r},\vec{r}')J_s(y')ds \tag{A-5}$$

The integration is over the surface of the probe at z=o, and $J_s(y) = I(y)/W$, where I(y) is given by (21). The Green's function $G(\vec{r},\vec{r}')$ can be expressed [4] in the following form

$$G(\vec{r},\vec{r}') = -\frac{1}{ab}\sum_{n=1}^{\infty}\sum_{m=o}^{\infty}\frac{(2-\delta_{om})}{\Gamma_{nm}}\sin\left(\frac{n\pi x}{a}\right)\sin\left(\frac{n\pi x'}{a}\right)\cdot$$

$$\cdot\cos\left(\frac{m\pi y}{b}\right)\cos\left(\frac{n\pi y'}{b}\right)\left[\exp\{-\Gamma_{nm}|z|\}-\exp\{-\Gamma_{nm}(2L+z)\}\right]$$

$$\text{where} \quad \Gamma_{nm} = \left[(n\pi/a)^2+(m\pi/b)^2-K_o^2\right]^{1/2} . \tag{A-6}$$

In this case (see Eq. (24)) the input impedance Z_{in} is given by

$$Z_{in} = -1/2 \iint_s E_y(x,y,o)\, J_s^*(y')ds/[1/2|J_s(o)|^2] \qquad (A-7)$$

The field E_y can be calculated using (A-2a), (A-5) and (A-6). Then carrying out the operation indicated in (A-7), the expression for the input impedance of an off-centered flat rectangular probe in a rectangular waveguide can be written in the following form.

$$Z_{in} = -\frac{jZ_oK_o \tan^2\left(\frac{K_od}{2}\right)}{ab} \sum_{n=1}^{\infty} \sum_{m=o}^{\infty} \frac{(2-\delta_{om})}{\Gamma_{nm}} \left[\frac{F_{1m}S_{1n}}{\hat{k}_m} \sin\left(\frac{n\pi d_1}{a}\right)\right]^2$$

$$\cdot[1-\exp\{-2\Gamma_{nm}L\}] \qquad (A-8)$$

where

$$F_{1m} = 1 - [\sin\left(\frac{m\pi d}{2b}\right)/\sin\left(\frac{K_od}{2}\right)]^2 \qquad (A-9a)$$

$$S_{1n} = \sin\left(\frac{n\pi w}{2a}\right)/\left(\frac{n\pi w}{2a}\right) \qquad (A-9b)$$

$$\hat{K}_m^2 = (m\pi/b)^2 - K_o^2 \qquad (A-9c)$$

When the probe is at the center of the broad dimension of the waveguide, i.e., when $d_1=a/2$, the expression for Z_{in} becomes

$$Z_{in} = -\frac{jZ_o K_o \tan^2(K_o d/2)}{ab} \sum_{n=o}^{\infty} \sum_{m=o}^{\infty} \frac{(2-\delta_{om})}{\gamma_{nm}} [1-\exp\{-2\gamma_{nm}L\}] \cdot$$

$$\cdot [F_{1m} \hat{S}_{1n} / \hat{K}_m]^2 \qquad \text{(A-10)}$$

where

$$\gamma_{nm} = [\{(2n+1)\pi/a\}^2 + \hat{K}_m^2]^{1/2} \qquad \text{(A-11a)}$$

$$\hat{S}_{1n} = \sin\{(2n-1)\pi/a\} / \{(2n+1)\pi/a\} \qquad \text{(A-11b)}$$

Note that the expression (A-10) is identical to the relation (30) which was obtained as a special case of an infinite linear array of probes inside a parallel plate waveguide. Furthermore, when $d_1=a/3$ or $d_1=2\,a/3$, then (A-8) becomes identical to (25) for some specific scan angle and frequency as mentioned in Section V-C. This will be demonstrated via numerical results. It may be reminded that neglect of the gap-effect and the assumption of known current distribution are the usual approximations made here.

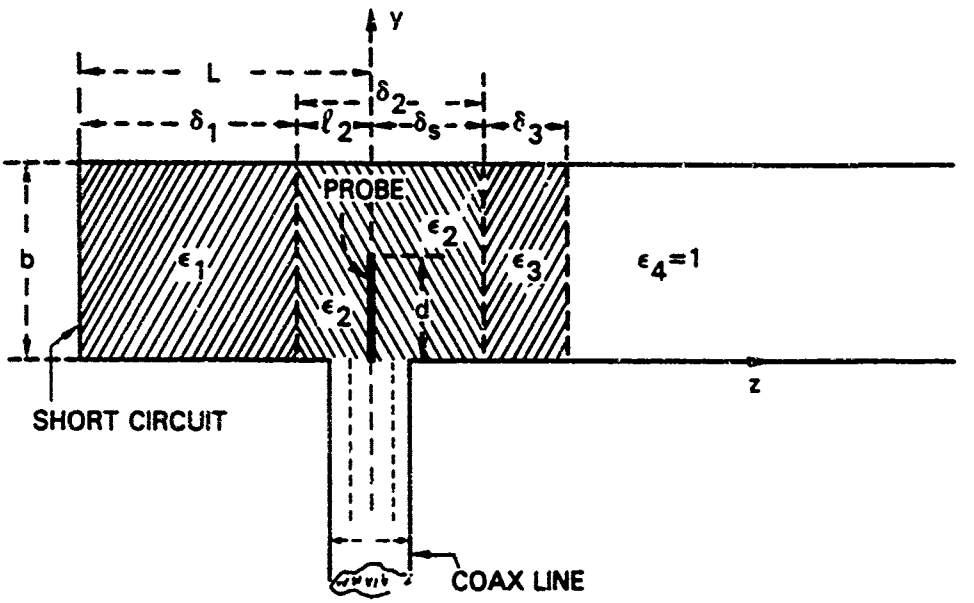

PARALLEL PLATE WAVEGUIDE [SIDE VIEW]

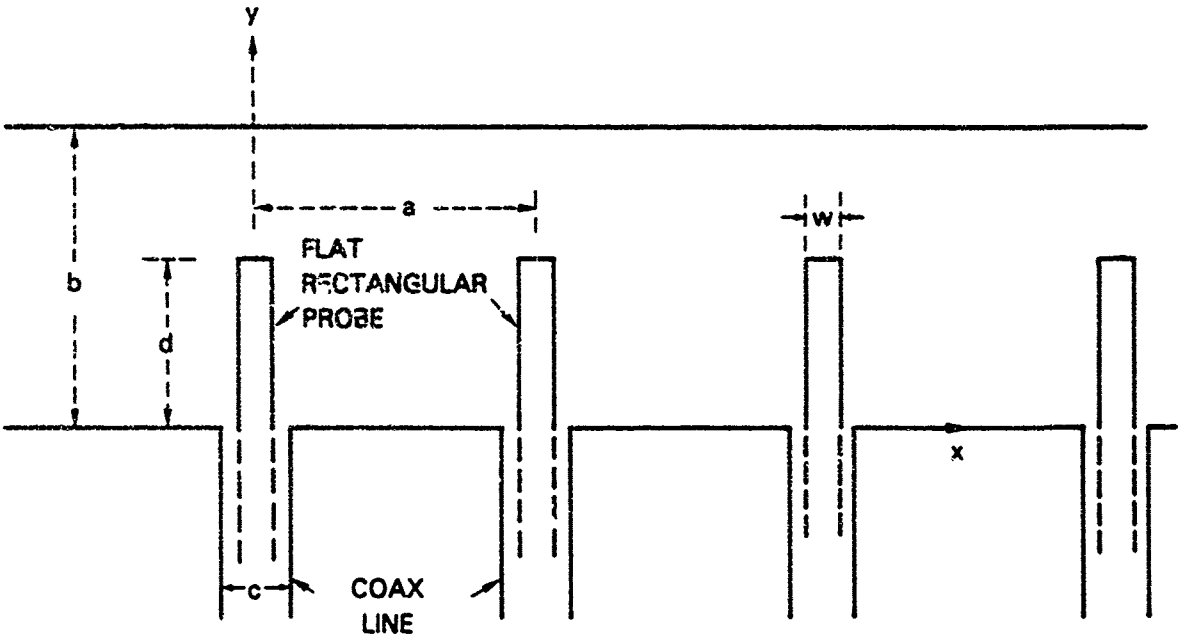

Fig. 1 — Linear array of flat rectangular probes in a parallel plate waveguide for H-plane scanning.

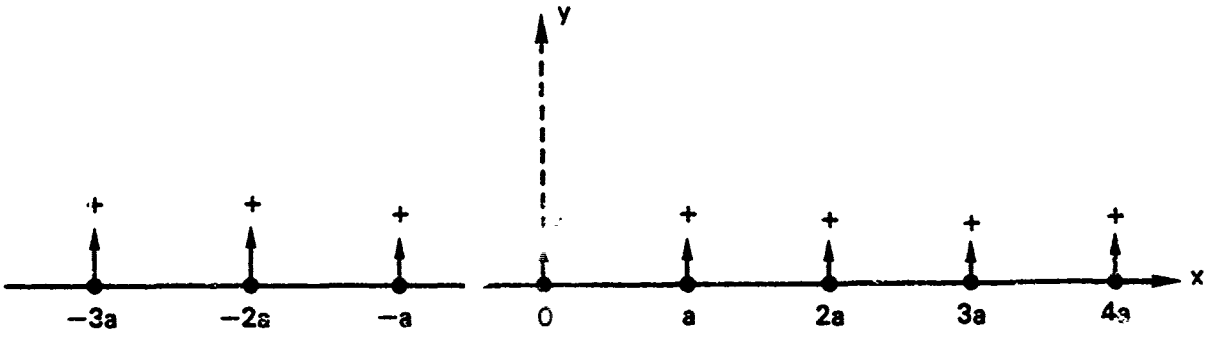

Fig. 2a — Schematic arrangement of probes as in Fig. 1.

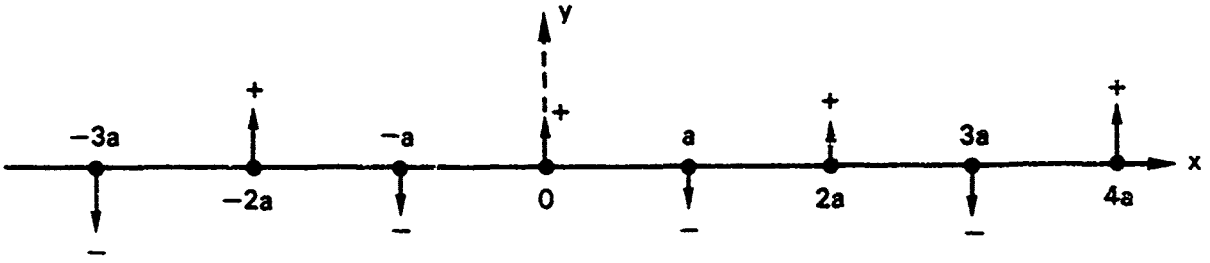

Fig. 2b — Probes having adjacent phases 180° apart.

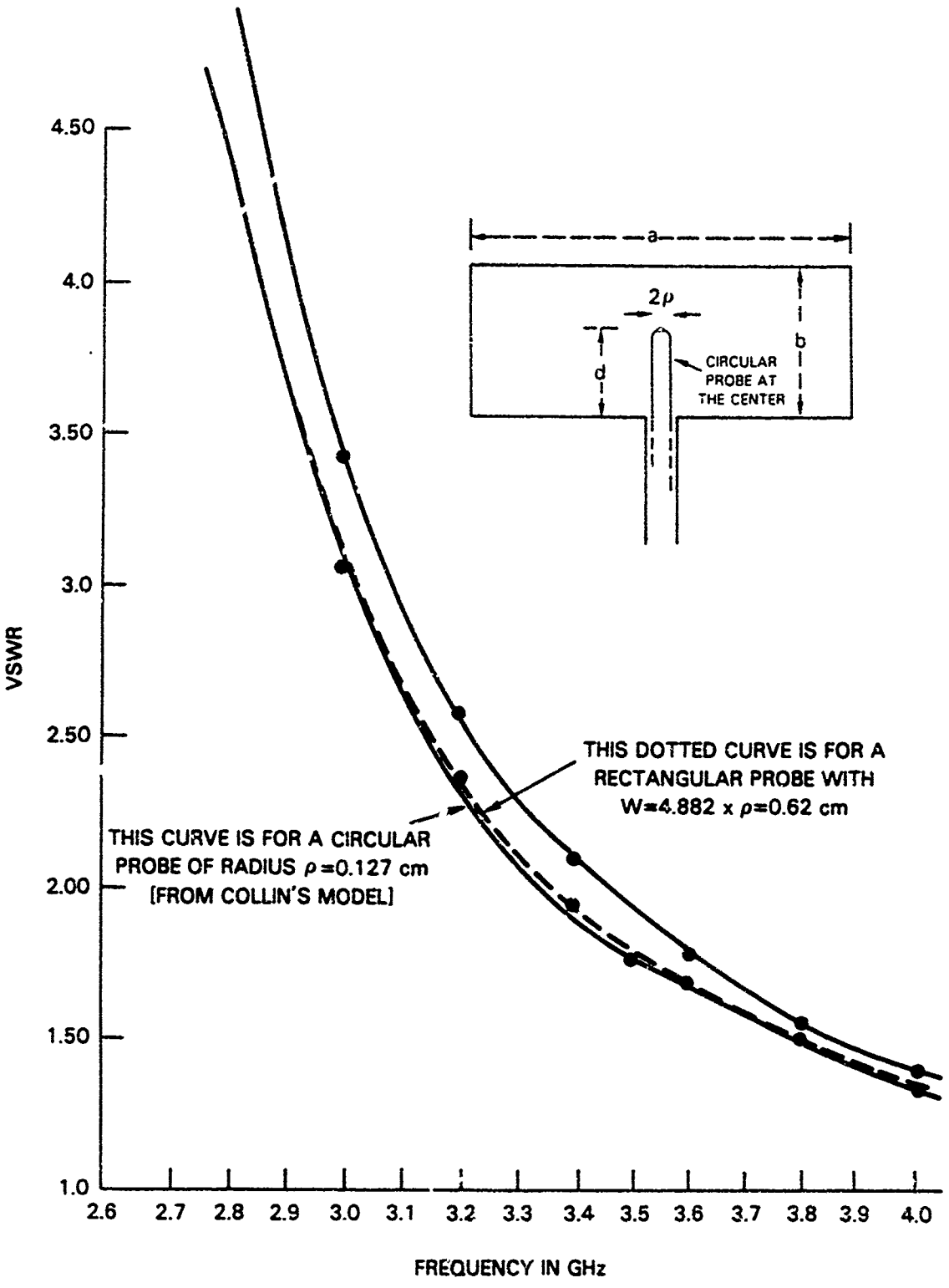

Fig. 3a — Connection between circular and flat rectangular probes in a rectangular waveguide.

$a = 2.362 \cdot (2.54)$ cm, $b = 1.34 \cdot (2.54)$ cm,
$L = 0.871 \cdot (2.54)$ cm, $\rho = 0.05 \cdot (2.54)$ cm,
and $d = 0.65 \cdot (2.54)$ cm.

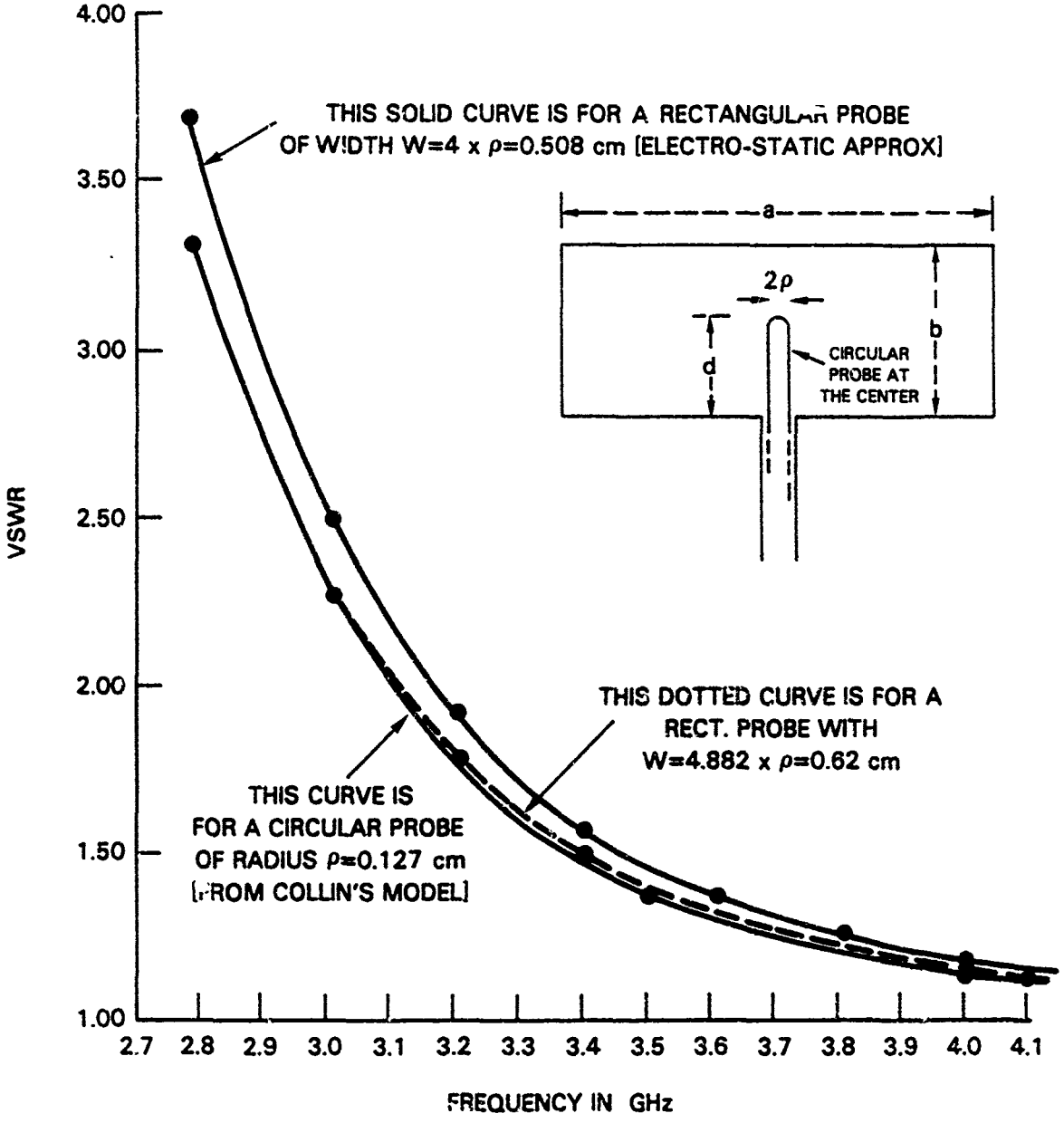

Fig. 3b — Connection between circular and flat rectangular probes in a rectangular waveguide.

$a = 2.362 \cdot (2.54)$ cm, $b = 1.34 \cdot (2.54)$ cm,
$L = 0.871 \cdot (2.54)$ cm, $\rho = 0.05 \cdot (2.54)$ cm,
and $d = 0.689 \cdot (2.54)$ cm.

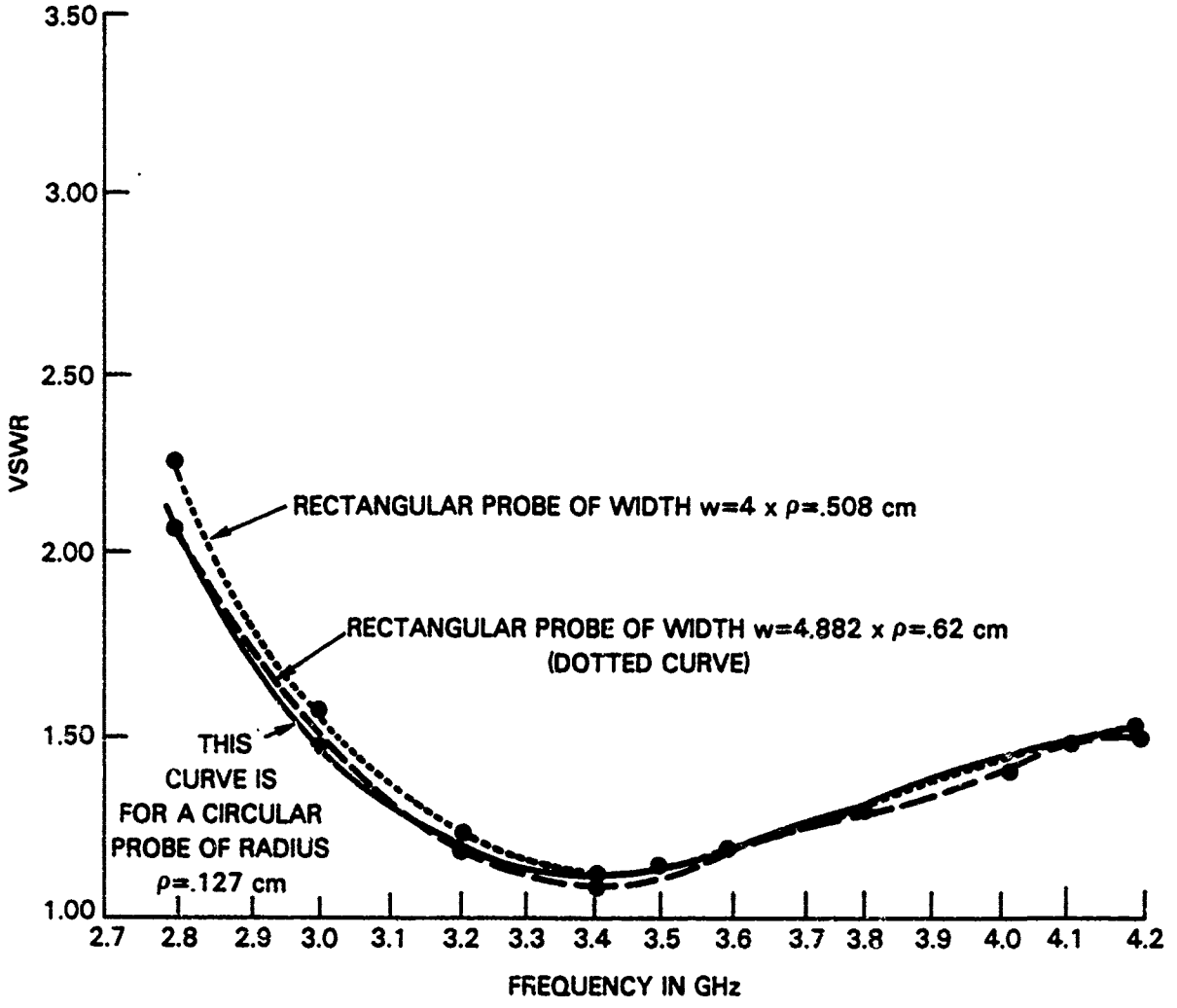

Fig. 3c — Connection between circular and flat rectangular probes in a rectangular waveguide.

$a = 2.362 \cdot (2.54)$ cm, $b = 1.34 \cdot (2.54)$ cm,
$L = 0.871 \cdot (2.54)$ cm, $\rho = 0.05 \cdot (2.54)$ cm,
and $d = 0.748 \cdot (2.54)$ cm.

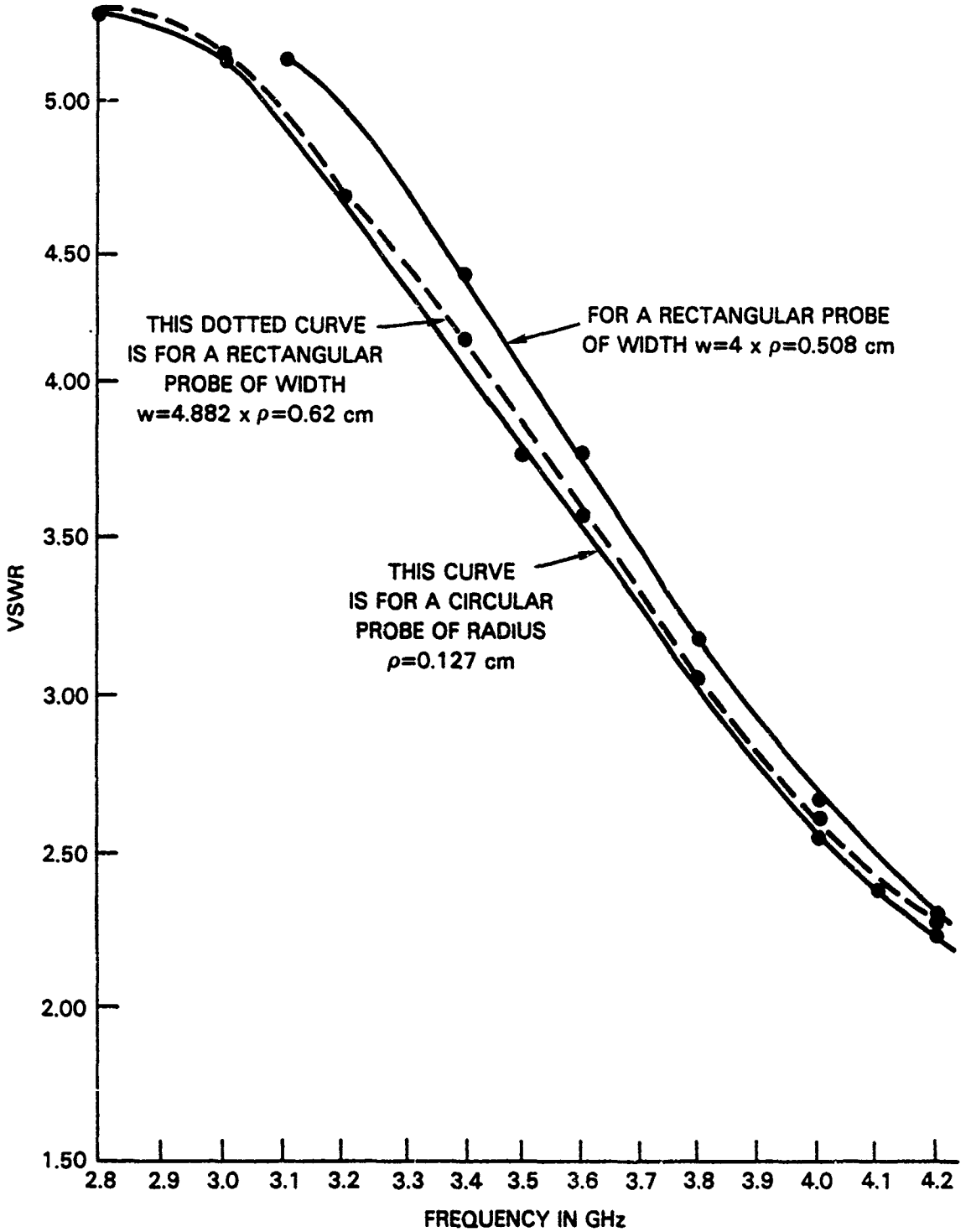

Fig. 4a — Connection between circular and flat rectangular probes in a rectangular waveguide.

$a = 2.362 \cdot (2.54)$ cm, $b = 1.34 \cdot (2.54)$ cm,
$L = \infty$, $\rho = 0.05 \cdot (2.54)$ cm,
and $d = 0.65 \cdot (2.54)$ cm.

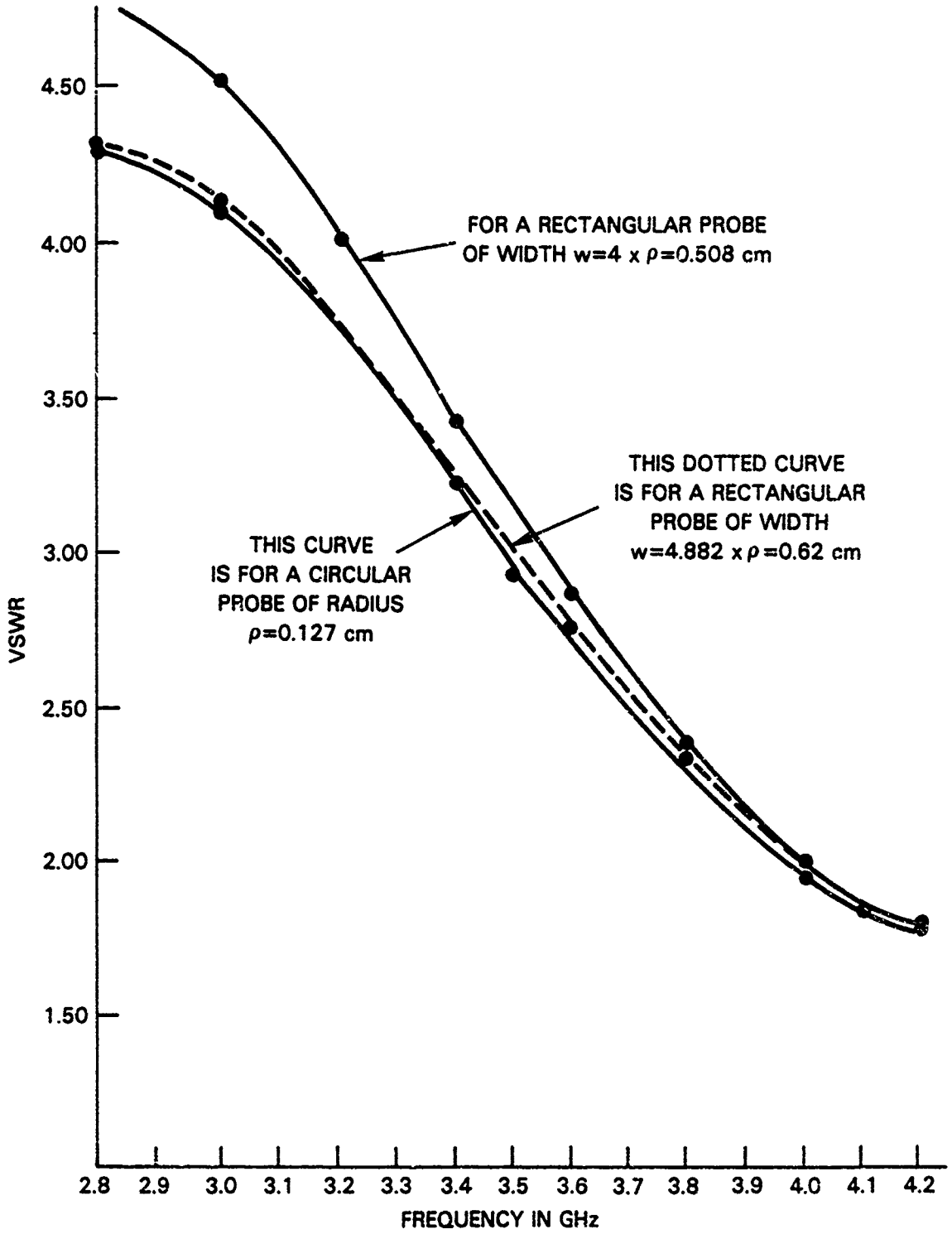

Fig. 4b — Connection between circular and flat rectangular probes in a rectangular waveguide.

$a = 2.362 \cdot (2.54)$ cm, $b = 1.34 \cdot (2.54)$ cm,
$L = \infty$, $\rho = 0.05 \cdot (2.54)$ cm,
and $d = 0.689 \cdot (2.54)$ cm.

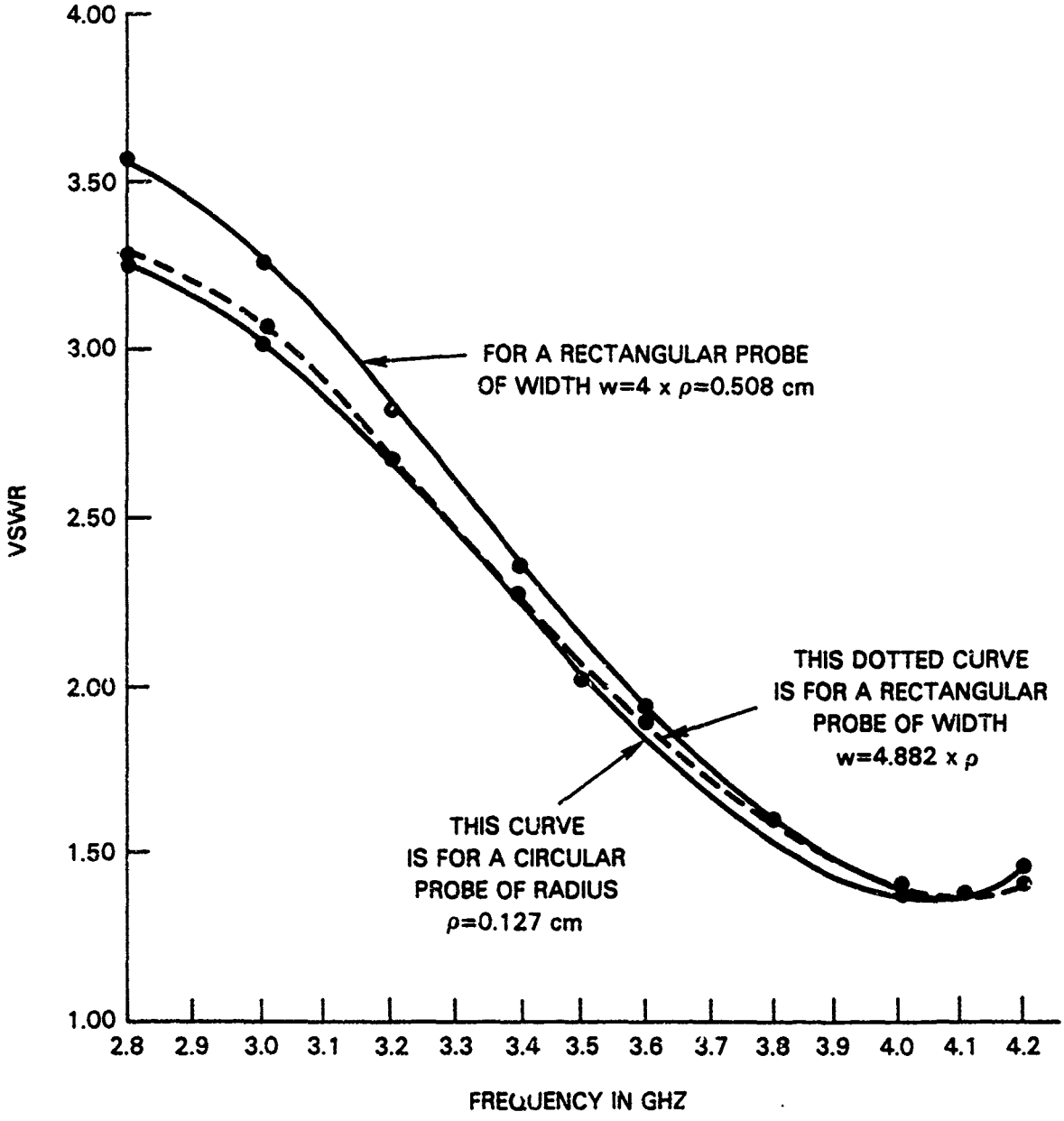

Fig. 4c — Connection between circular and flat rectangular probes in a rectangular waveguide.

$a = 2.362 \cdot (2.54)$ cm, $b = 1.34 \cdot (2.54)$ cm,
$L = \infty$, $\rho = 0.05 \cdot (2.54)$ cm,
and $d = 0.748 \cdot (2.54)$ cm.

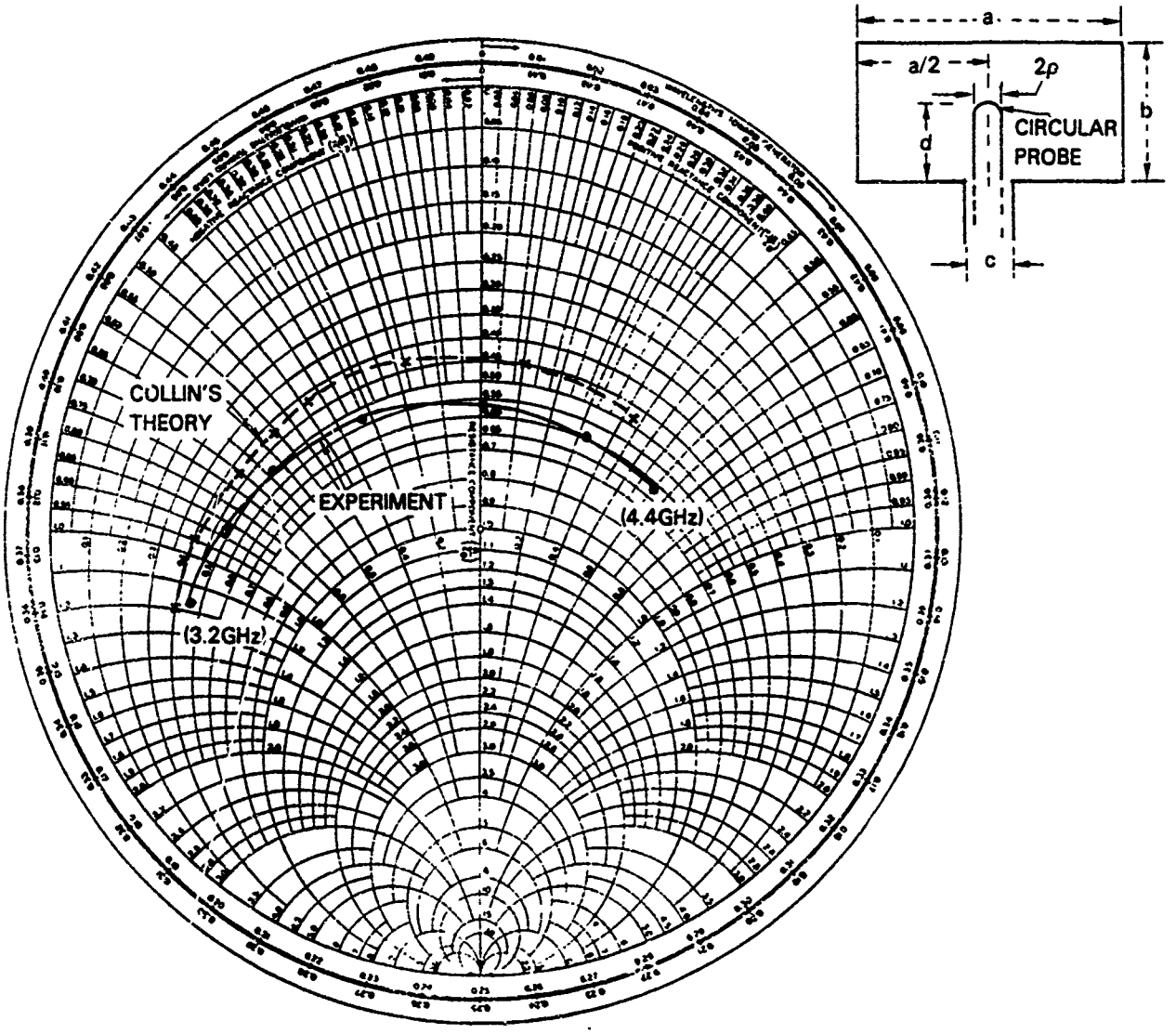

Fig. 5a — Impedance of a circular probe in an infinitely long rectangular waveguide.

$a = 2.84 \cdot (2.54)$ cm, $b = 1.34 \cdot (2.54)$ cm,
$d = 0.70 \cdot (2.54)$ cm, $2\rho = 0.049 \cdot (2.54)$ cm,
and $c = 0.163 \cdot (2.54)$ cm.

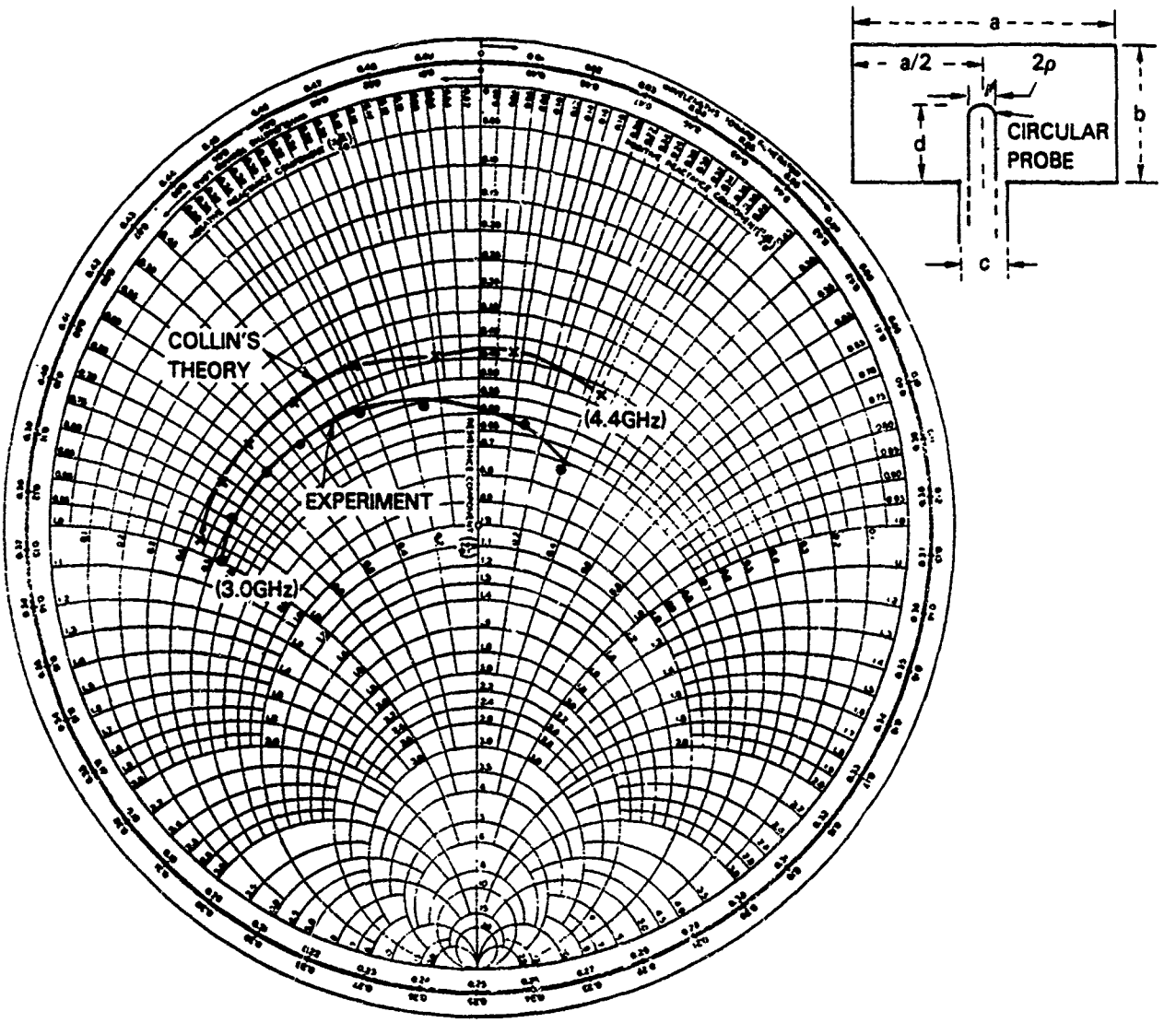

Fig. 5b — Impedance of a circular probe in an infinitely long rectangular waveguide.

$a = 2.84 \cdot (2.54)$ cm, $b = 1.34 \cdot (2.54)$ cm,
$d = 0.70 \cdot (2.54)$ cm, $2\rho = 0.125 \cdot (2.54)$ cm,
and $c = 0.360 \cdot (2.54)$ cm.

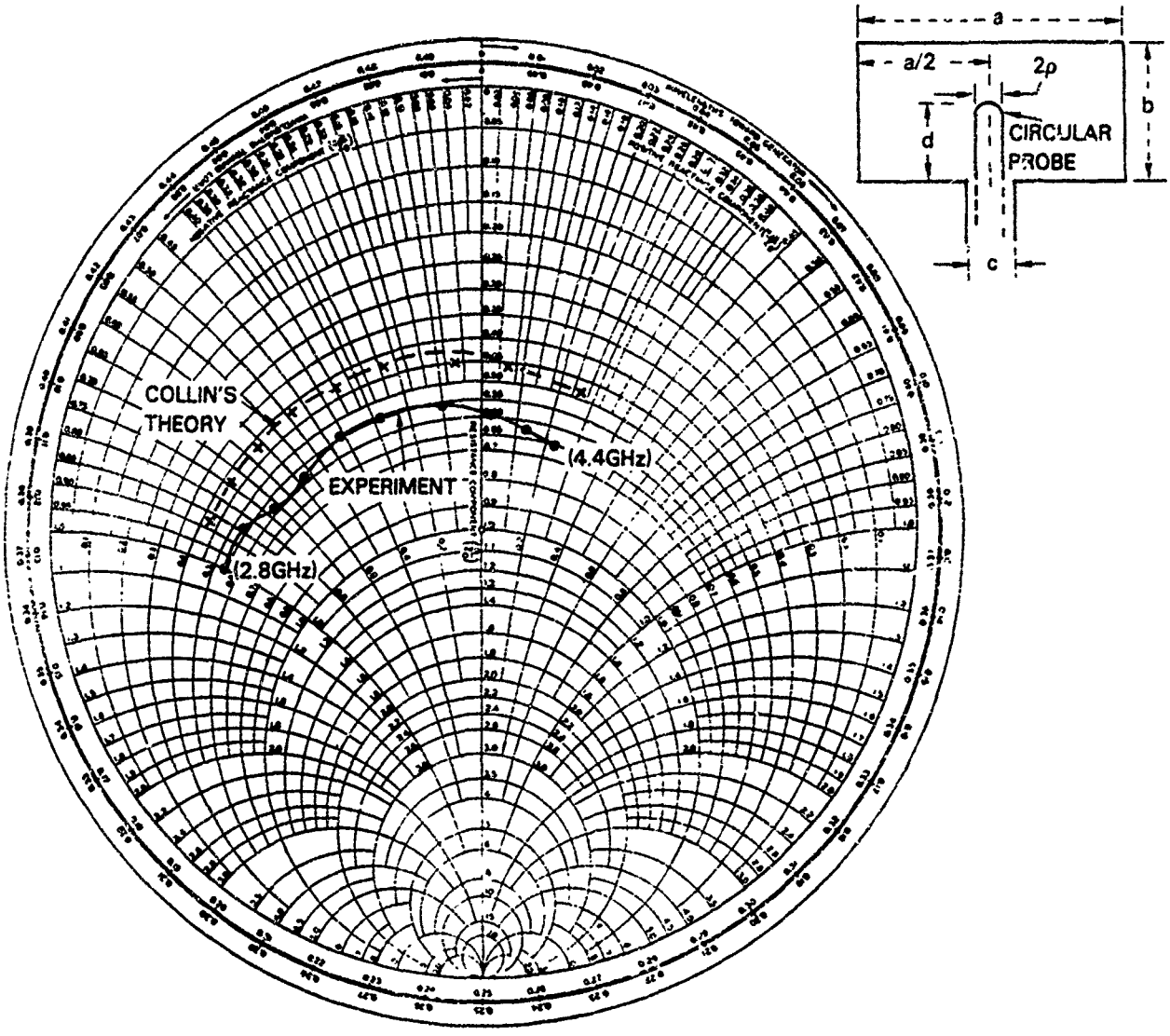

Fig. 5c — Impedance of a circular probe in an infinitely long rectangular waveguide.

$a = 2.84 \cdot (2.54)$ cm, $b = 1.34 \cdot (2.54)$ cm,
$d = 0.70 \cdot (2.54)$ cm, $2\rho = 0.20 \cdot (2.54)$ cm,
and $c = 0.456 \cdot (2.54)$ cm.

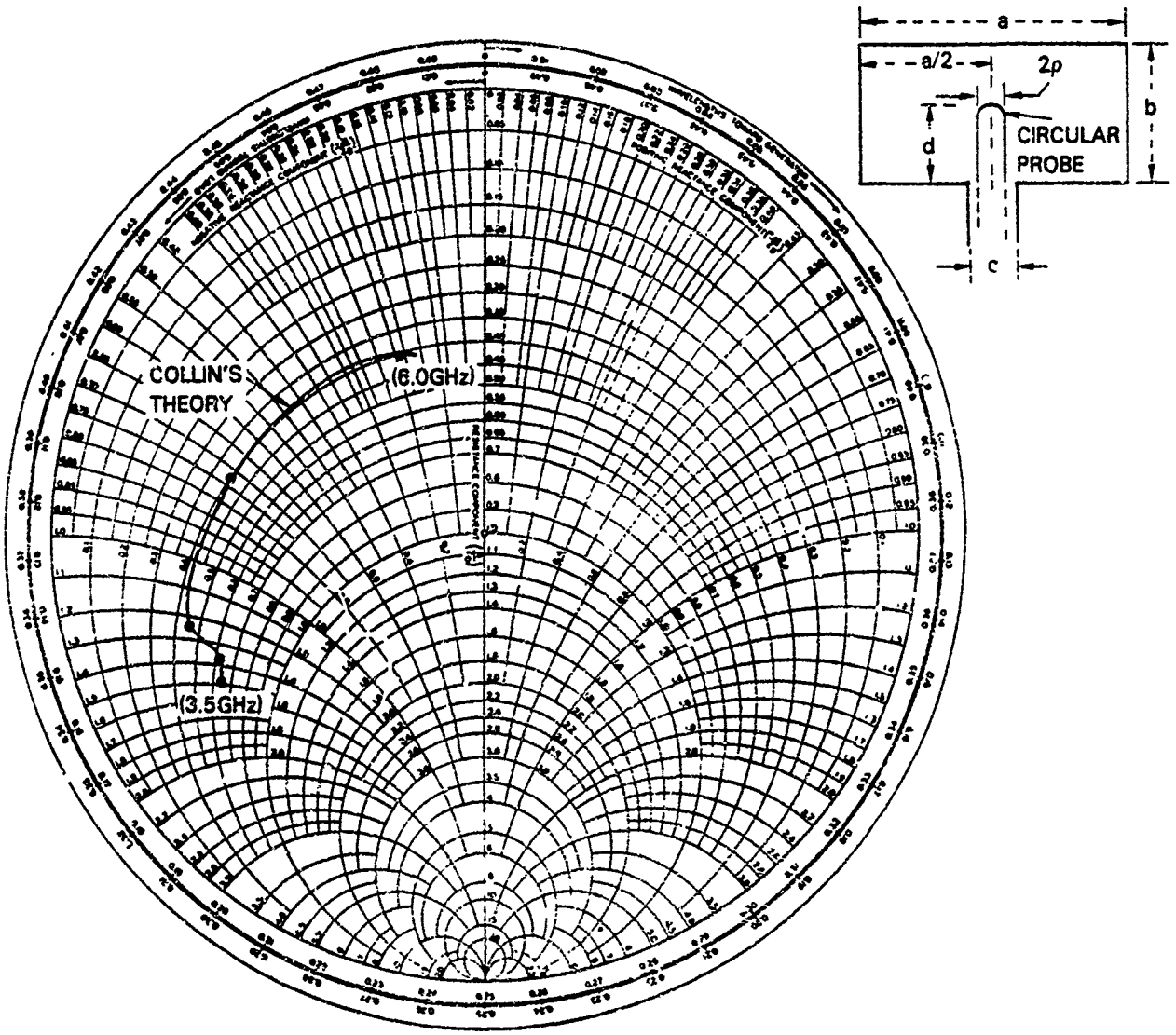

Fig. 5d — Impedance of a circular probe in an infinitely long rectangular waveguide.

a = 4.76 cm, b = 2.22 cm,
d = 1.15 cm, 2ρ = 0.23 cm,
and c = 1.10 cm.

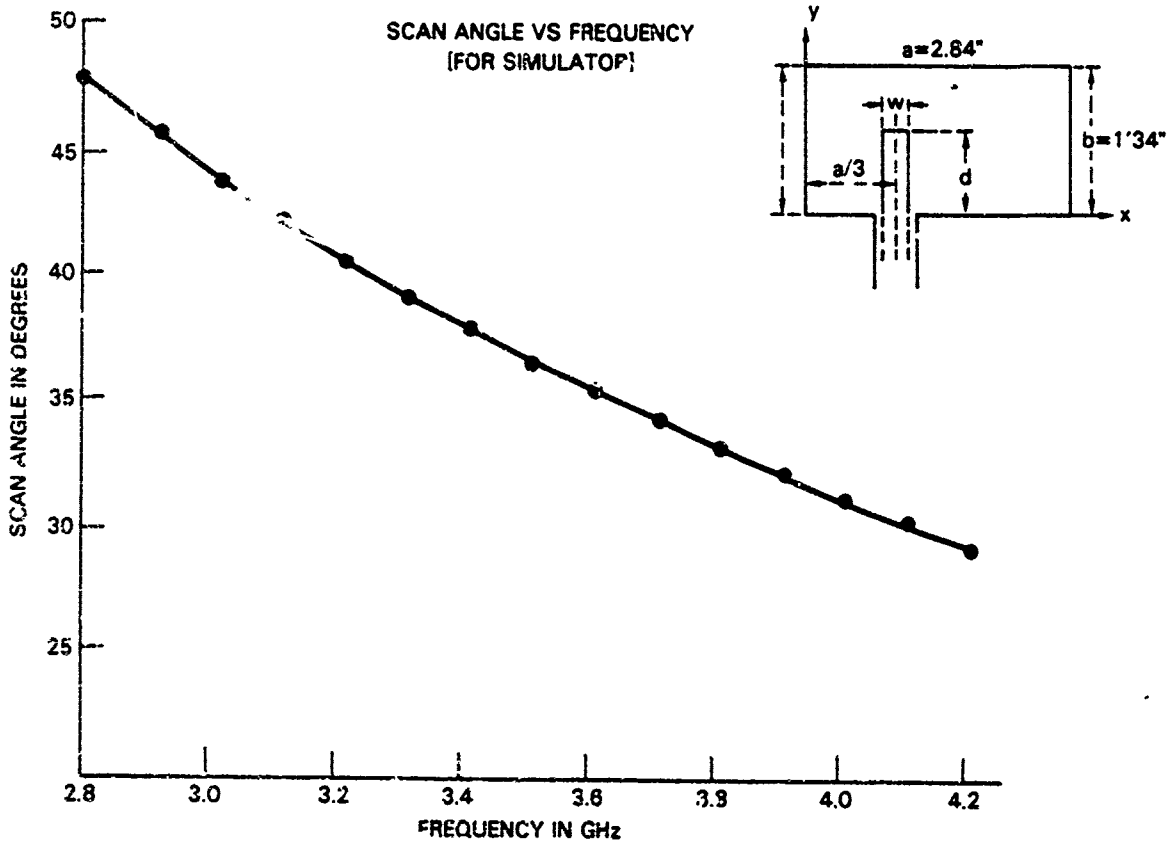

Fig. 6a -- Scan angle vs Frequency [for a simulator].

$a = 2.84 \cdot (2.54)$ cm,
$b = 1.34 \cdot (2.54)$ cm,
$d_1 = a/3$.

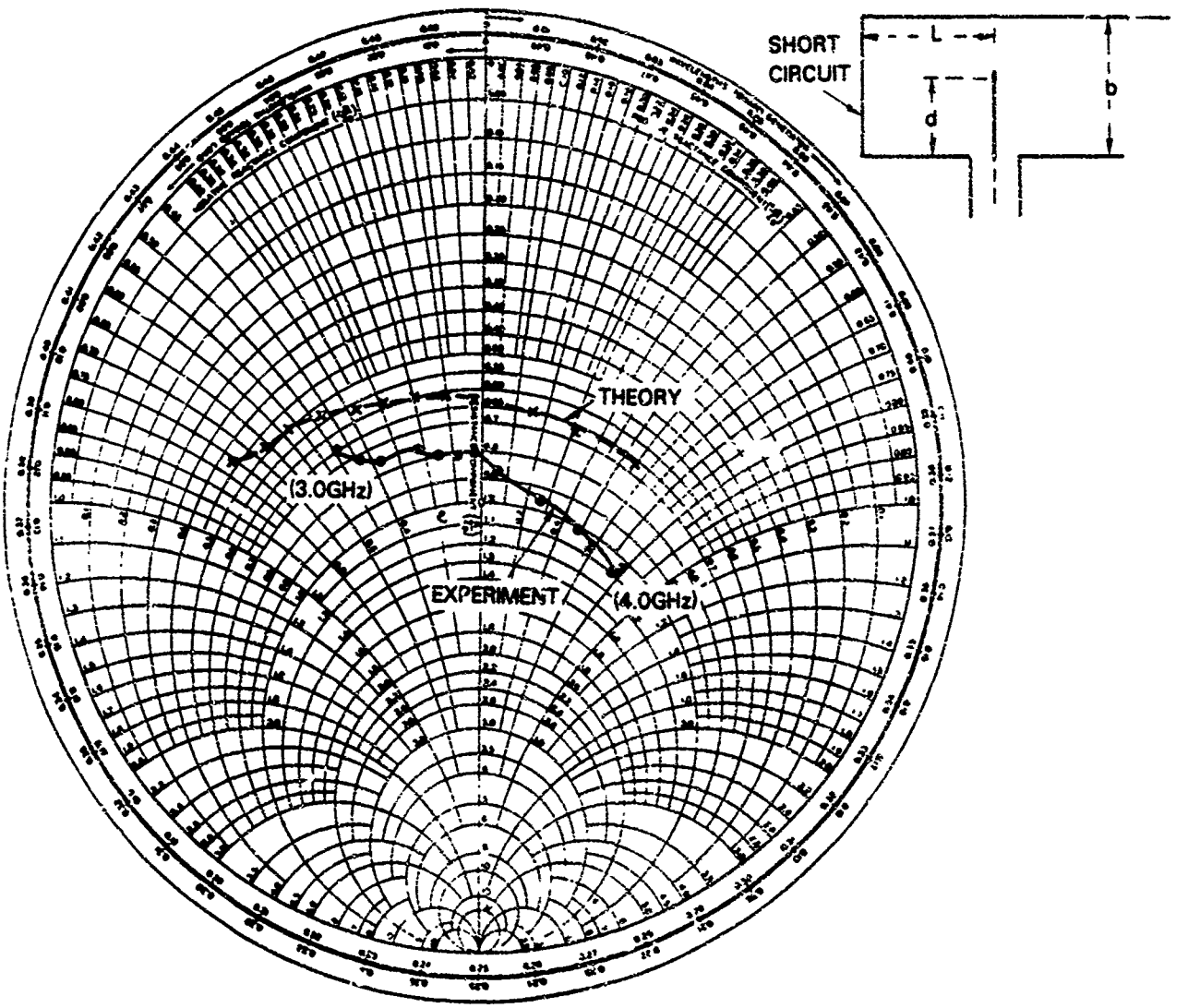

Fig. 6b — Array impedance in S-band simulator—Offset flat probes without dielectric sheet.
$\epsilon_1 = \epsilon_2 = \epsilon_3 = \epsilon_4 = 1$, $a = 2.84 \cdot (2.54)$ cm $= 3d_1$,
$b_1 = 1.34 \cdot (2.54)$ cm, $w = 0.2 \cdot (2.54)$ cm,
$d = 0.702 \cdot (2.54)$ cm, and $L = 0.863 \cdot (2.54)$ cm.

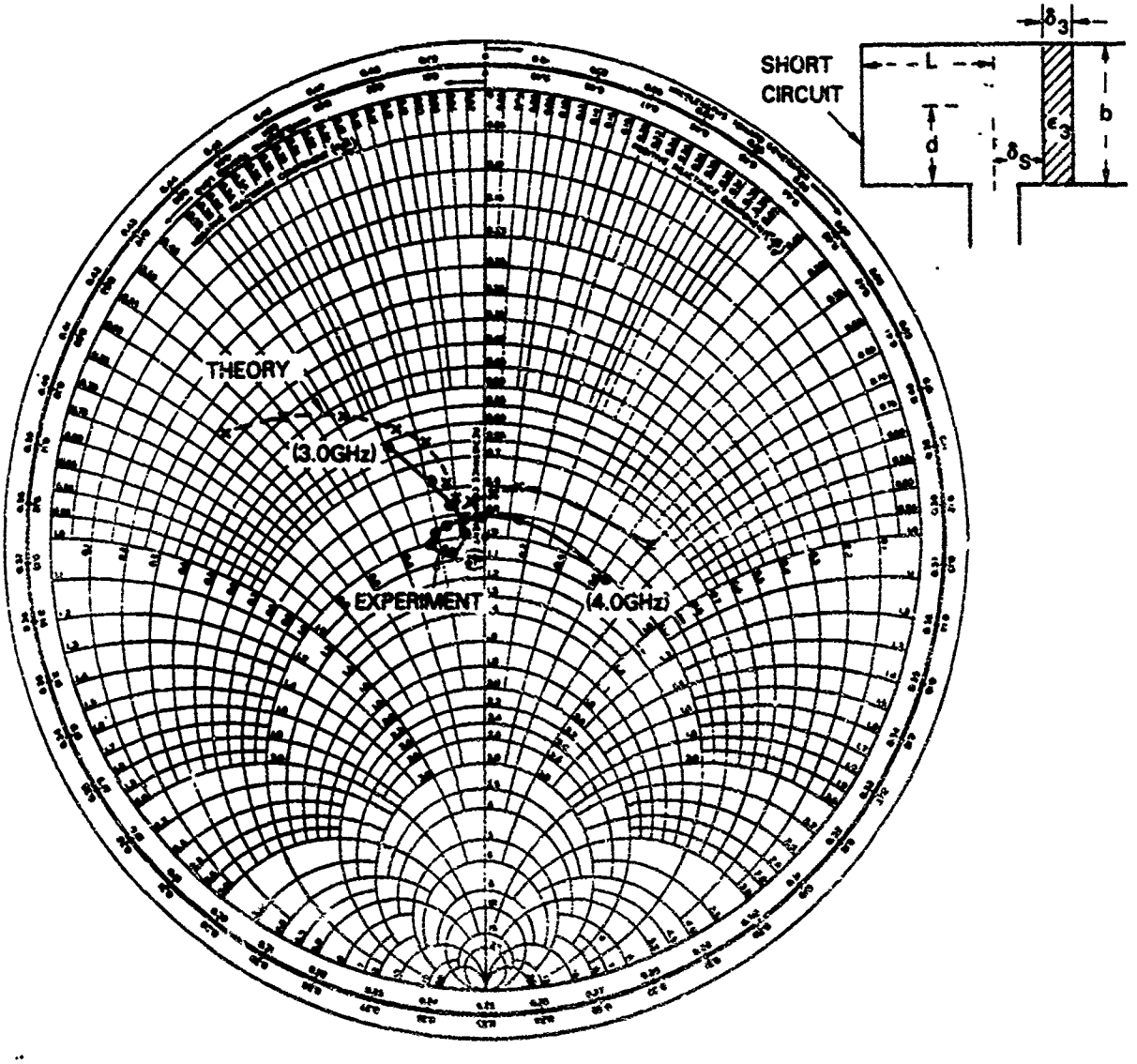

Fig. 6c — Array impedance in S-band simulator—Offset flat probe with dielectric sheet.
$\epsilon_1 = \epsilon_2 = \epsilon_4 = 1$, $\epsilon_3 = 1.3$, $a = 2.84 \cdot (2.54)$ cm $= 3d_1$,
$b_1 = 1.34 \cdot (2.54)$ cm, $w = 0.2 \cdot (2.54)$ cm, $d = 0.702 \cdot (2.54)$ cm,
$L = 0.863 \cdot (2.54)$ cm, $\delta_s = 0.984 \cdot (2.54)$ cm, $\delta_3 = 1.0 \cdot (2.54)$ cm

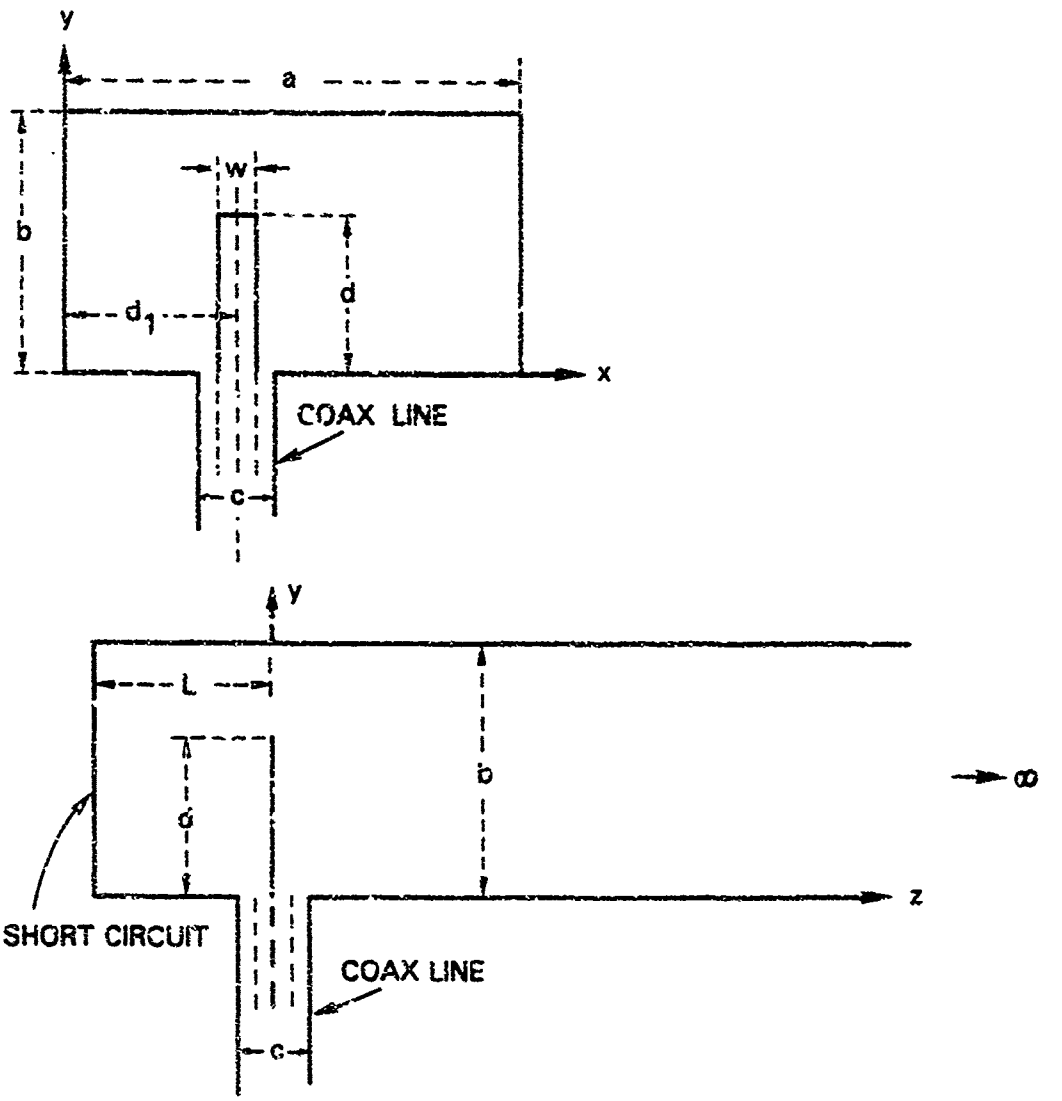

Fig. A-1 — Offset flat rectangular probe in a rectangular waveguide.